

Double-layer Heisenberg antiferromagnet at finite temperature: Brueckner theory and quantum Monte Carlo simulations

P. V. Shevchenko,^a A. W. Sandvik,^b and O. P. Sushkov ^a

^a *School of Physics, The University of New South Wales, Sydney 2052, Australia*

^b *Department of Physics, University of Illinois at Urbana-Champaign, Urbana, Illinois 61801*

(October 30, 2018)

Abstract

The double-layer Heisenberg antiferromagnet with intra- and inter-layer couplings J and J_{\perp} exhibits a zero temperature quantum phase transition between a quantum disordered dimer phase for $g > g_c$ and a Neel phase with long range antiferromagnetic order for $g < g_c$, where $g = J_{\perp}/J$ and $g_c \approx 2.5$. We consider the behavior of the system at finite temperature for $g \geq g_c$ using two different and complementary approaches; an analytical Brueckner approximation and numerically exact quantum Monte Carlo simulations. We calculate the temperature dependent spin excitation spectrum (including the triplet gap), dynamic and static structure factors, the specific heat, and the uniform magnetic susceptibility. The agreement between the analytical and numerical approaches is excellent. For $T \rightarrow 0$ and $g \rightarrow g_c$, our analytical results for the specific heat and the magnetic susceptibility coincide with those previously obtained within the nonlinear σ model approach for $N \rightarrow \infty$. Our quantum Monte Carlo simulations extend to significantly lower temperatures than previously, allowing us to obtain accurate results for the asymptotic quantum critical behavior. We also obtain an improved estimate for the critical coupling: $g_c = 2.525 \pm 0.002$.

PACS numbers: 75.10.Jm, 75.30.Kz, 75.50Ee

I. INTRODUCTION

The Heisenberg antiferromagnet on a double-layer square lattice has become an important model for studying quantum antiferromagnetism in two dimensions. It was introduced by Millis and Monien as a phenomenological model to capture the spin-gap behavior observed in high- T_c compounds such as $\text{YBa}_2\text{Cu}_3\text{O}_{6+x}$,^{1,2} in which the basic structural unit is a pair of CuO_2 planes. The Heisenberg bilayer with inter- and intra-layer couplings J and J_\perp can be tuned through an antiferromagnetic order-disorder transition at zero temperature by varying the ratio $g = J_\perp/J$. For $g < g_c$ there is long-range antiferromagnetic order at zero temperature, whereas for $g > g_c$ the tendency to singlet formation across the layers leads to a disordered ground state and a spin gap. The critical ratio $g_c \approx 2.5$ has been determined using a variety of numerical methods.^{3–5} The inter-layer coupling in bilayer cuprates is typically much smaller than this value; neutron scattering experiments indicate $g \approx 0.1$ in $\text{YBa}_2\text{Cu}_3\text{O}_6$.⁶ Although experimental realizations of antiferromagnetic bilayers with $g \approx g_c$ are currently lacking, the model in this regime is important for theoretical investigations of quantum critical and quantum disordered behavior.⁷

It has been argued by Haldane⁸ and Chakravarty, Halperin and Nelson⁹ that the $T = 0$ quantum phase transition in two-dimensional quantum antiferromagnets is described by the 2+1-dimensional nonlinear $O(3)$ σ -model, and therefore the universality class should be that of the 3D classical Heisenberg model. The nonlinear σ -model has three distinct regimes in the $T-g$ plane near the quantum critical point. For $g < g_c$ the long-range antiferromagnetic order at $T = 0$ is destroyed by thermal fluctuations for any $T > 0$. At low temperatures, in the so-called renormalized classical regime, the correlation length diverges exponentially as $T \rightarrow 0$; $\xi \propto e^{2\pi\rho_s/T}$, where ρ_s is the spin stiffness. For $g > g_c$ the singlet-triplet excitation gap implies a low-temperature quantum disordered regime where the correlation length is temperature independent and remains finite as $T \rightarrow 0$. Exactly at g_c , ρ_s vanishes and the correlation length diverges as $1/T$. This is the leading behavior also in the high-temperature quantum critical regime for both $g < g_c$ and $g > g_c$. Exactly at $g = g_c$, the quantum critical regime extends down to $T = 0$, whereas for $g \neq g_c$ there is a crossover to either renormalized classical or quantum disordered behavior at lower temperature.

The mapping of the Heisenberg model to the nonlinear σ -model has been rigorously proven only for the single-layer square lattice antiferromagnet with nearest-neighbor interactions,⁸ which itself does not exhibit a zero-temperature quantum phase transition. Assuming the σ -model description, the universal dynamic and static properties of two-dimensional antiferromagnets in the vicinity of a zero-temperature phase transition have been studied in detail by Sachdev, Ye, and Chubukov^{10,11} using an $1/N$ expansion ($N = 3$ is the number of components of the σ -model). They found that close to criticality, many physical observables such as the specific heat, the magnetic susceptibility, e.t.c., depend in a universal manner on a small number of model dependent parameters. The Heisenberg bilayer is an ideal model to numerically test these predictions.⁴ The model is not frustrated, and therefore the “sign problem” hampering simulations of the single-layer J_1 - J_2 model is not present. Compared to other dimerized models, the bilayer has the advantage that the square lattice symmetry in the planes is not broken, and therefore the asymptotic behavior should be more easily observed.¹²

The zero-temperature transition of the bilayer system has been well studied by various

numerical methods, including dimer-series expansions by Hida³ and Zheng,⁵ and quantum Monte Carlo simulations by Sandvik and Scalapino.⁴ These studies determined the critical point in the range be $g_c \approx 2.50 - 2.56$. The scaling behavior is consistent with 3D Heisenberg critical exponents.

The finite temperature properties have been also extensively studied by numerical methods. Quantum Monte Carlo simulations were performed by Sandvik and collaborators^{4,13} and showed a reasonably good agreement with the predicted quantum critical behavior. High-temperature expansions were carried out by Oitmaa *et al.*¹⁴ and finite-cluster exact diagonalisation was used by Jaklic and Prelovsek.¹⁵ Finally, high-order strong-coupling thermodynamic expansions for this model were developed by Elstner and Singh.¹⁶ Unfortunately, all the methods have so far been restricted to relatively high temperatures. A particular recent concern is that the strong-coupling expansions by Elstner and Singh indicate a change in the behavior of the susceptibility and the specific heat close to the lowest temperature considered in the Monte Carlo simulations.¹⁶ It is not clear whether this is due to the breakdown of the combined high-temperature and strong-coupling expansion, which is expected at low temperature, or if the Monte Carlo results do not reflect the true asymptotic quantum critical regime.

On the analytical side, until recently the progress with the bilayer model was less impressive because the conventional spin-wave theory used by Hida³ and the Schwinger boson mean field approach applied by Millis and Monien¹ were not able to take into account in an appropriate way the strong interactions between elementary triplets. These approaches yielded results which were inconsistent with the numerical studies. In particular, a much too high critical coupling $g_c \approx 4.5$ was obtained. A more sophisticated treatment by Chubukov and Morr,¹⁷ taking into account longitudinal spin fluctuations which are important close to g_c , gave an improved value $g_c \approx 2.7$ and was also able to explain other aspects of the quantum Monte Carlo results.

A very efficient analytical approach to deal with a dimerized disordered quantum spin system at zero temperature has recently been developed by Kotov *et al.*¹⁸ This method is based on the same ideas as the Brueckner theory of nuclear matter,¹⁹ and we therefore call it the “Brueckner method”. This approach has already led to rather spectacular success in several problems, including a calculation of g_c (yielding $g_c = 2.60$), the zero temperature critical index, and the excitation spectrum for the bilayer model,^{18,20} the elementary excitation spectrum and bound states for one-dimensional spin-ladders and spin chains^{21,22}, as well as the ground state structure and the excitation spectrum of the frustrated two-dimensional $J_1 - J_2$ model.²³

One of the purposes of the present work is to develop a generalization of the Brueckner method to the case of finite temperature, using as a testing ground the Heisenberg bilayer Hamiltonian. All analytical results are general, however, and can be applied to any dimerized quantum spin system, including one-dimensional spin ladders and chains. In the present paper we focus on the quantum disordered and quantum critical regimes of the bilayer. Our formulas can be formally extended to the renormalized classical regime, but in that case there are very important corrections that we plan to consider in a future study.

In order to test the reliability of this new theoretical approach, we have also carried out quantum Monte Carlo simulations at considerably lower temperatures than before. This allows us to definitely conclude that the asymptotic quantum critical regime has been reached,

and to resolve the above mentioned questions arising from strong-coupling expansions. The simulations also give an improved estimate of the critical coupling; $g_c = 2.525 \pm 0.002$.

Using the Brueckner method, we have calculated the temperature dependent spectrum of excitations, dynamic and static structure factors and susceptibilities, the specific heat, and the uniform magnetic susceptibility. In the limit $T \rightarrow 0$, $g \rightarrow g_c$, our results for the correlation length, the specific heat, and the magnetic susceptibility coincide with those previously obtained using $N \rightarrow \infty$ calculations for the nonlinear σ -model.^{10,11} The Monte Carlo approach gives numerically exact results for the thermodynamics. The agreement with the analytical calculations is excellent at low temperature ($T/J \lesssim 0.5$). Using sum rules, we can also extract an approximate excitation spectrum from the quantum Monte Carlo results. Also in this case the agreement with the theory is very good.

The rest of the paper is organized as follows. In Sec. II we first summarize the main steps of the Brueckner approach at zero temperature, and then proceed to the new calculations at finite temperature. In Sec. III we discuss the Monte Carlo simulations and present data allowing us to extract an accurate value for g_c . We also discuss finite-size effects. We present comparisons between analytical and numerical results for various physical quantities in Sec. IV. In Sec. V we summarize and discuss our main conclusions.

II. BRUECKNER THEORY

The double-layer Heisenberg model we study is defined by the Hamiltonian

$$H = J \sum_{\langle i,j \rangle} (\mathbf{S}_{1i} \cdot \mathbf{S}_{1j} + \mathbf{S}_{2i} \cdot \mathbf{S}_{2j}) + J_{\perp} \sum_i \mathbf{S}_{1i} \cdot \mathbf{S}_{2i}, \quad (1)$$

where $S_{a,i}$ is a spin-1/2 operator at site i of layer a ($a = 1, 2$), $\langle i, j \rangle$ denotes a pair of nearest-neighbor sites on the square lattice, and the total number of sites in a layer is L^2 . Both the coupling constants are antiferromagnetic, i.e., $J, J_{\perp} > 0$. In Sec. II-A we summarize the main steps of the Brueckner diagrammatic approach developed in Refs. 18,20 for this model at zero temperature. In Sec. II-B we generalize the approach to $T > 0$.

A. Zero temperature

Our approach is formulated in the basis of bond singlets and triplets. We define a creation operator $t_{\alpha i}^{\dagger}$ for a triplet ($S = 1$) with polarization $\alpha = x, y, z$ at bond i , where i connects two nearest-neighbor spins $\mathbf{S}_1(i)$ and $\mathbf{S}_2(i)$. In the bond operator representation^{24,25}

$$S_{1,2}^{\alpha}(i) = \frac{1}{2}(\pm t_{\alpha} \pm t_{\alpha}^{\dagger} - i\epsilon_{\alpha\beta\gamma} t_{\beta}^{\dagger} t_{\gamma}), \quad (2)$$

and one can exactly map the Hamiltonian (1) to the effective Hamiltonian

$$H_{\text{eff}} = H_2 + H_4 + H_U, \quad (3)$$

where

$$H_2 = \sum_{\alpha,i} J_{\perp} t_{\alpha i}^{\dagger} t_{\alpha i} + \frac{\lambda J}{2} (t_{\alpha i}^{\dagger} t_{\alpha i+1} + t_{\alpha i}^{\dagger} t_{\alpha i+1}^{\dagger} + h.c), \quad (4a)$$

$$H_4 = \frac{J}{2} \sum_{\langle i,j \rangle, \alpha, \beta} (t_{\alpha i}^{\dagger} t_{\beta j}^{\dagger} t_{\beta i} t_{\alpha j} - t_{\alpha i}^{\dagger} t_{\alpha j}^{\dagger} t_{\beta i} t_{\beta j}), \quad (4b)$$

$$H_U = U \sum_{i, \alpha, \beta} t_{\alpha i}^{\dagger} t_{\beta i}^{\dagger} t_{\beta i} t_{\alpha i}, \quad U \rightarrow \infty, \quad (4c)$$

Hereafter we set $\lambda = 1$, except at the end of Sec. II-B where it will be convenient to use a variable λ to formally separate the contributions from quadratic and quartic terms in the Hamiltonian.

At the quadratic level the Hamiltonian (3) can be diagonalized by a combination of Fourier,

$$t_{\mathbf{k}, \alpha}^{\dagger} = \frac{1}{L} \sum_{\mathbf{r}} t_{\mathbf{r}, \alpha}^{\dagger} e^{i(\mathbf{k} + \mathbf{k}_0)\mathbf{r}}, \quad \mathbf{k}_0 = (\pi, \pi), \quad (5)$$

and Bogoliubov,

$$t_{\mathbf{k}\alpha} = u_{\mathbf{k}} a_{\mathbf{k}\alpha} + v_{\mathbf{k}} a_{-\mathbf{k}\alpha}^{\dagger}, \quad (6)$$

transformations. This gives the excitation spectrum

$$\tilde{\omega}_{\mathbf{k}}^2 = A_{\mathbf{k}}^2 - B_{\mathbf{k}}^2, \quad (7)$$

where

$$A_{\mathbf{k}} = J_{\perp} + 2J\xi_{\mathbf{k}}, \quad (8a)$$

$$B_{\mathbf{k}} = 2J\xi_{\mathbf{k}}, \quad (8b)$$

and

$$\xi_{\mathbf{k}} = -(\cos k_x + \cos k_y)/2. \quad (9)$$

The momentum takes values within the Brillouin zone $-\pi < k_x, k_y \leq \pi$, but for convenience we have shifted the argument in the Fourier transform (5) by $\mathbf{k}_0 = (\pi, \pi)$. In this notation the minimum of the spin-wave dispersion is at $\mathbf{k} = 0$.

An infinite on-site repulsion between triplets, H_U , has been introduced in order to take into account the hard-core constraint $t_{\alpha i}^{\dagger} t_{\beta i}^{\dagger} = 0$ (only one triplet can be excited on a bond). For $g \gtrsim g_c \approx 2.5$, the contribution of the quartic term H_4 is relatively small and H_U therefore gives the dominant contribution to the renormalization of the spin-wave spectrum. Since H_U is infinite the exact scattering amplitude

$$\Gamma_{\alpha\beta,\gamma\delta} = \Gamma(\mathbf{K})(\delta_{\alpha\gamma}\delta_{\beta\delta} + \delta_{\alpha\delta}\delta_{\beta\gamma}), \quad (10)$$

where $\mathbf{K} = (\mathbf{k}, \omega)$ is the total energy and momentum of the incoming particles, can be found from the following equation, which is diagrammatically represented in Figure 1(a),

$$\Gamma(\mathbf{K}) = - \left(\frac{1}{L^2} \sum_{\mathbf{p}} \frac{u_{\mathbf{p}}^2 u_{\mathbf{k}-\mathbf{p}}^2}{\omega - \omega_{\mathbf{p}} - \omega_{\mathbf{k}-\mathbf{p}}} \right)^{-1}. \quad (11)$$

The Bogoliubov coefficients are

$$u_{\mathbf{k}}^2, v_{\mathbf{k}}^2 = \pm 1/2 + A_{\mathbf{k}}/(2\omega_{\mathbf{k}}). \quad (12)$$

The basic approximation made in the derivation of $\Gamma(\mathbf{K})$ is the neglect of all anomalous scattering vertices which are present in the theory due to existence of the anomalous Green's function,

$$G_a(\mathbf{k}, t) = -i\langle T(t_{-\mathbf{k}\alpha}^\dagger(t)t_{\mathbf{k}\alpha}^\dagger(0)) \rangle. \quad (13)$$

The crucial observation is that all anomalous contributions are suppressed by a small parameter of the theory — the density of triplet excitations,

$$\rho = \langle t_{\alpha i}^\dagger t_{\alpha i} \rangle = \frac{3}{L^2} \sum_{\mathbf{q}} v_{\mathbf{q}}^2. \quad (14)$$

It was found in Ref. 18 that $\rho \approx 0.12$ at the critical point, $g = g_c$, and that ρ decreases as g increases.

The normal self-energy corresponding to the scattering amplitude $\Gamma(\mathbf{K})$ is given by the equation shown diagrammatically in Figure 1(b):

$$\Sigma(\mathbf{k}, \omega) = \frac{4}{L^2} \sum_{\mathbf{q}} v_{\mathbf{q}}^2 \Gamma(\mathbf{k} + \mathbf{q}, \omega - \omega_{\mathbf{q}}). \quad (15)$$

In order to find the renormalized spectrum, one has to solve the coupled Dyson equations for the normal Green's function

$$G_n(\mathbf{k}, t) = -i\langle T(t_{\mathbf{k}\alpha}(t)t_{\mathbf{k}\alpha}^\dagger(0)) \rangle \quad (16)$$

and the anomalous (13). Further separation into a quasiparticle contribution and incoherent background yields

$$\omega_{\mathbf{k}} = Z_{\mathbf{k}} \sqrt{\tilde{A}_{\mathbf{k}}^2 - \tilde{B}_{\mathbf{k}}^2}, \quad (17)$$

where

$$\tilde{A}_{\mathbf{k}} = J_{\perp} + 2J\xi_{\mathbf{k}} + \Sigma(\mathbf{k}, 0) + 4J\xi_{\mathbf{k}} \frac{1}{L^2} \sum_{\mathbf{q}} \xi_{\mathbf{q}} v_{\mathbf{q}}^2, \quad (18a)$$

$$\tilde{B}_{\mathbf{k}} = 2J\xi_{\mathbf{k}} - 4J\xi_{\mathbf{k}} \frac{1}{L^2} \sum_{\mathbf{q}} \xi_{\mathbf{q}} u_{\mathbf{q}} v_{\mathbf{q}}. \quad (18b)$$

We also define

$$Z_{\mathbf{k}} = \left(1 - \frac{\partial \Sigma}{\partial \omega} \Big|_{\omega=0} \right)^{-1}, \quad (19)$$

and

$$U_{\mathbf{k}}^2, V_{\mathbf{k}}^2 = \frac{Z_{\mathbf{k}} \tilde{A}_{\mathbf{k}}}{2\omega_{\mathbf{k}}} \pm \frac{1}{2}. \quad (20)$$

The renormalized coefficients $\tilde{A}_{\mathbf{k}}$ and $\tilde{B}_{\mathbf{k}}$ (18) also take into account the quartic interaction (4b) in the one-loop approximation because the corresponding effect is small. In order to find the spectrum, equations (11),(15), and (17)-(20) with the substitutions

$$u_{\mathbf{k}} \rightarrow \sqrt{Z_{\mathbf{k}}}U_{\mathbf{k}}, \quad v_{\mathbf{k}} \rightarrow \sqrt{Z_{\mathbf{k}}}V_{\mathbf{k}} \quad (21)$$

have to be solved self-consistently for $\Sigma(\mathbf{k}, 0)$ and $Z_{\mathbf{k}}$.

The results of the self-consistent solution for the spin-wave gap, $\Delta_0 = \omega_{k=0}$, are in excellent agreement with a dimer series expansions¹⁸ even close to the critical point, as shown in Figure 2. The value of the critical coupling is $g_c \approx 2.60$, only slightly larger than the numerically determined value $g_c = 2.51 \pm 0.02$.⁴ It has been demonstrated in Ref. 20 that the Brueckner approximation itself results in a critical behavior for the triplet gap, $\Delta_0 \sim (g - g_c)^\nu$, with critical index $\nu = 1/2$. It was also shown that for the model under consideration the actual small parameter is $\rho \ln(J/\Delta_0)$. Thus when the gap is very small the approach can fail. Nevertheless, the critical behavior of the gap can be analyzed analytically (see Ref. 20) by expanding the Brueckner equations in powers of the triplet density ρ . In the leading approximation the contribution from the quasiparticle residue to the renormalization (21) can be neglected and we have to set $u_{\mathbf{k}}^2 = 1$ in the vertex (11):

$$\Gamma(\mathbf{q}, -\omega_{\mathbf{q}}) = \left(\int \frac{d^2\mathbf{p}}{(2\pi)^2} \frac{1}{\omega_{\mathbf{q}} + \omega_{\mathbf{p}} + \omega_{\mathbf{p}-\mathbf{q}}} \right)^{-1}. \quad (22)$$

Then the variation of the self-energy (15) with the deviation $\delta g = g - g_c$ results in a linear relation between gap, Δ_0 , and δg near the critical point:

$$\Delta_0/J \approx a(g - g_c), \quad (23)$$

where the constant $a \approx 1.1$ has been evaluated in Ref. 20. The critical exponent $\nu = 1$ corresponding to (23) is the same as the one predicted within the nonlinear σ model for $N \rightarrow \infty$.¹¹ The plot of the gap, $\Delta_0(g)$, obtained from the self-consistent solution of low-density Brueckner equations, i.e., the solution of Eqs. (15) and (17)-(20) together with the vertex (22) [and the substitutions $u_{\mathbf{k}}, v_{\mathbf{k}} \rightarrow U_{\mathbf{k}}, V_{\mathbf{k}}$] is also shown in Figure 2. The resulting value of the critical coupling, $g_c \approx 2.32$, is about 10% lower than numerically determined one.

Consideration of the first correction due to the finite triplet density, i.e. using $u_{\mathbf{p}}^2 u_{\mathbf{k}-\mathbf{p}}^2 = (1 + v_{\mathbf{p}}^2)(1 + v_{\mathbf{k}-\mathbf{p}}^2) \approx 1 + v_{\mathbf{p}}^2 + v_{\mathbf{k}-\mathbf{p}}^2$ in the vertex (11), results in a logarithmic correction at small momenta, $\Gamma(q, -\omega_q) \approx \Gamma_c(1 + \beta \ln q)$, and yields

$$\Delta_0/J = a\delta g(1 - \beta \ln \delta g), \quad (24)$$

with the constant $\beta \approx 0.3$ evaluated in Ref. 20. Assuming scaling behavior, $\Delta_0 \sim (\delta g)^\nu$, the logarithmic correction results in a critical index, $\nu = 1 - \beta \approx 0.67 \pm 0.03$, which agrees with numerical studies and the prediction of the σ model ($\nu \approx 0.70$). This concludes the solution of the two-layer Heisenberg antiferromagnet at zero temperature.

B. Finite temperature

Having described in the previous section the Brueckner method at zero temperature as a starting point, we next consider the bilayer Heisenberg antiferromagnet at finite temperature. The generalization of the method to $T > 0$ is simple because in essence it is a low-density approximation. Thus it is convenient to use the Feynman technique instead of the Matsubara one. In this approximation they are equivalent to each other.

Only the normal Green's function $G_n(\mathbf{k}, t) = -i\langle T(a_{\mathbf{k}\alpha}(t)a_{\mathbf{k}\alpha}^\dagger(0)) \rangle$ exists for physical operators $a_{\mathbf{k}\alpha}$. At finite temperature in an ideal gas approximation, it can be written via retarded and advanced functions, $G^{R,A}(\mathbf{k}, \omega) = [\omega - \omega_{\mathbf{k}} \pm i0]^{-1}$, as (see Ref. 26)

$$G_n(\mathbf{k}, \omega) = \frac{1}{2}[G^R + G^A] + \frac{1}{2}\text{ctanh}\frac{\omega}{2T}[G^R - G^A]. \quad (25)$$

Then, after Fourier (5) and Bogoliubov (6) transformations the normal and anomalous Green's functions

$$G_n^T(\mathbf{k}, t) = -i\langle T(t_{k\alpha}(t)t_{k\alpha}^\dagger(0)) \rangle, \quad (26a)$$

$$G_a^T(\mathbf{k}, t) = -i\langle T(t_{-k\alpha}^\dagger(t)t_{k\alpha}^\dagger(0)) \rangle, \quad (26b)$$

at finite temperature are

$$G_n^T(\mathbf{k}, \omega) = \frac{u_{\mathbf{k}}^2(1+n_{\mathbf{k}})}{\omega - \omega_{\mathbf{k}} + i0} - \frac{u_{\mathbf{k}}^2 n_{\mathbf{k}}}{\omega - \omega_{\mathbf{k}} - i0} - \frac{v_{\mathbf{k}}^2(1+n_{\mathbf{k}})}{\omega + \omega_{\mathbf{k}} - i0} + \frac{v_{\mathbf{k}}^2 n_{\mathbf{k}}}{\omega + \omega_{\mathbf{k}} + i0}, \quad (27)$$

$$G_a^T(\mathbf{k}, \omega) = u_{\mathbf{k}}v_{\mathbf{k}} \left(\frac{1+n_{\mathbf{k}}}{\omega - \omega_{\mathbf{k}} + i0} - \frac{n_{\mathbf{k}}}{\omega - \omega_{\mathbf{k}} - i0} + \frac{n_{\mathbf{k}}}{\omega + \omega_{\mathbf{k}} + i0} - \frac{1+n_{\mathbf{k}}}{\omega + \omega_{\mathbf{k}} - i0} \right), \quad (28)$$

where $n_{\mathbf{k}} = \langle a_{\mathbf{k},\alpha}^\dagger a_{\mathbf{k},\alpha} \rangle = (e^{\omega_{\mathbf{k}}/T} - 1)^{-1}$ with no summation over α . The essential feature is that despite the bosonic commutation relations of the single triplet operators, these do not have conventional bosonic distribution function because of the strong interactions. Actually, $\omega_{\mathbf{k}}$ is a functional of $n_{\mathbf{k}}$, and thus the expression $n_{\mathbf{k}} = (e^{\omega_{\mathbf{k}}/T} - 1)^{-1}$ should be considered as an implicit definition of the thermal distribution function $n_{\mathbf{k}}$. The density of triplet excitations, trivially obtained from the normal Green's function (27) at finite temperature, is given by

$$\begin{aligned} \rho^T &= \langle t_{i\alpha}^\dagger t_{i\alpha} \rangle = i \cdot \lim_{\tau \rightarrow -0} \frac{3}{L^2} \sum_{\mathbf{q}} \int G_n^T(\mathbf{k}, \omega) e^{-i\omega\tau} \frac{d\omega}{2\pi} \\ &= \frac{3}{L^2} \sum_{\mathbf{q}} (v_{\mathbf{q}}^2(1+n_{\mathbf{q}}) + u_{\mathbf{q}}^2 n_{\mathbf{q}}). \end{aligned} \quad (29)$$

Our approach is valid for low density of triplet excitations, and therefore our consideration is restricted to low temperatures; $T < J_\perp, J$. We will take into account only leading temperature corrections to the self energy (15) neglecting temperature corrections to the vertex (22). The quantum transition disappears at any finite temperature and there is only a disordered phase with a finite gap towards to triplet excitations. Thus we expect that the low-density Brueckner equations is an appropriate tool for the model in the $g \geq g_c$ region, where the

neglected logarithmic corrections, $\rho \ln(\Delta_T/J)$ and $\rho \ln(\Delta_0/J)$ are not large and the vertex in the form (22) can be used. Using the normal time-dependant Green's function (27) for the diagram yields

$$\Sigma^T(\mathbf{k}, \omega) = \frac{4}{L^2} \sum_{\mathbf{q}} \left[v_{\mathbf{q}}^2 (1 + n_{\mathbf{q}}) \Gamma(\mathbf{k} + \mathbf{q}, \omega - \omega_{\mathbf{q}}) + u_{\mathbf{q}}^2 n_{\mathbf{q}} \Gamma(\mathbf{k} + \mathbf{q}, \omega + \omega_{\mathbf{q}}) \right]. \quad (30)$$

In order to find the renormalized spectrum at finite temperature, one has to solve the coupled Dyson equations for the normal and anomalous Green's functions (27) and (28), as was done in Sec. II-A at zero temperature. Further separation into a quasiparticle contribution and incoherent background renormalizes the coefficients

$$\tilde{A}_{\mathbf{k}} = J_{\perp} + 2J\xi_{\mathbf{k}} + \Sigma^T(\mathbf{k}, 0) + 4J\xi_{\mathbf{k}} \frac{1}{L^2} \sum_{\mathbf{q}} \xi_{\mathbf{q}} [v_{\mathbf{q}}^2 (1 + n_{\mathbf{q}}) + u_{\mathbf{q}}^2 n_{\mathbf{q}}], \quad (31a)$$

$$\tilde{B}_{\mathbf{k}} = 2J\xi_{\mathbf{k}} - 4J\xi_{\mathbf{k}} \frac{1}{L^2} \sum_{\mathbf{q}} \xi_{\mathbf{q}} u_{\mathbf{q}} v_{\mathbf{q}} (1 + 2n_{\mathbf{q}}), \quad (31b)$$

where the effect due to H_4 is also taken into account in the the one-loop approximation. Then the finite temperature renormalized spectrum $\omega_{\mathbf{k}}$, the renormalization constant $Z_{\mathbf{k}}$, and the Bogoliubov coefficients $U_{\mathbf{k}}$ and $V_{\mathbf{k}}$ are given by Eqs. (17) and (20) with the self-energy (30) and the coefficients (31).

In the low-density approximation the equations (17),(19),(20),(22),(30), and (31) should be solved self-consistently for $\Sigma^T(\mathbf{k}, 0)$ and $Z(\mathbf{k})$ with the substitution $u_{\mathbf{k}} \rightarrow U_{\mathbf{k}}$, $v_{\mathbf{k}} \rightarrow V_{\mathbf{k}}$.

All thermodynamic functions of the system can be obtained from free energy \mathbf{F} . The total energy of the system can not be found as a simple summation of quasiparticle energies because of the strong interactions, but it can be calculated in following way: Assume that the parameter λ in the quadratic term (4a) takes values between 0 and 1. Then we have

$$\frac{\partial \mathbf{F}}{\partial \lambda} = \left\langle \frac{\partial H}{\partial \lambda} \right\rangle_T. \quad (32)$$

If $\lambda = 0$, the system is a set of dimers with free energy

$$\mathbf{F}_0 = -T \ln(1 + 3e^{-J_{\perp}/T}). \quad (33)$$

Integrating Eq. (32) then yields

$$\mathbf{F} - \mathbf{F}_0 = \int_0^1 d\lambda \left\langle \frac{\partial H}{\partial \lambda} \right\rangle_T, \quad (34)$$

where

$$\begin{aligned} \left\langle \frac{\partial H}{\partial \lambda} \right\rangle_T &= \frac{J}{2L^2} \sum_{i\alpha} \langle t_{\alpha i}^{\dagger} t_{\alpha i+1} + t_{\alpha i}^{\dagger} t_{\alpha i+1}^{\dagger} + \text{h.c.} \rangle \\ &= J \frac{6}{L^2} \sum_{\mathbf{k}} \xi_{\mathbf{k}} (v_{\mathbf{k}}^2 [1 + n_{\mathbf{k}}] + u_{\mathbf{k}}^2 n_{\mathbf{k}} + u_{\mathbf{k}} v_{\mathbf{k}} [1 + 2n_{\mathbf{k}}]). \end{aligned} \quad (35)$$

Using Eq. (34), one can calculate the thermodynamic potential and all thermodynamic functions using the self-consistent solution for the spectrum $\omega_{\mathbf{k}}$ and the Bogoliubov coefficients $v_{\mathbf{k}}^2$ and $u_{\mathbf{k}}^2$ at finite temperature.

This concludes the solution of the two-layer Heisenberg antiferromagnet model at finite temperature. The results of self-consistent solution of the Brueckner equations for the triplet gap, the spectrum, as well as various thermodynamic quantities will be presented in Sec. IV, along with comparisons with numerically exact results obtained using the quantum Monte Carlo method discussed in the next section.

III. QUANTUM MONTE CARLO

Quantum Monte Carlo simulations of the Heisenberg bilayer have previously been used to determine the $T = 0$ critical coupling, with the result $g = 2.51 \pm 0.02$.⁴ This value is also in good agreement with results obtained using dimer series expansion methods.^{3,5} Finite-temperature simulations in the quantum critical regime^{4,13} have shown generally good agreement with predictions of $1/N$ calculations for the nonlinear σ model. However, the algorithm used in the previous simulations did not work well at very low temperatures, and therefore there has been some concern¹⁶ that the results do not reflect the true $T \rightarrow 0$ behavior. Recently, the “stochastic series expansion” algorithm^{27,28} used in previous work has been considerably improved by the introduction²⁹ of a new cluster-type updating scheme (inspired by the “loop algorithms” developed for worldline Monte Carlo simulations³⁰) that overcomes the limitations of the previous local sampling scheme. We have used this algorithm for large-scale calculations in order to obtain a more precise estimate of the critical point and to study the low-temperature quantum critical and quantum disordered behavior. In this section we extract the $T = 0$ critical coupling and also discuss effects of finite lattice size in $T > 0$ calculations. In the Sec. IV we will compare results for the thermodynamics and the excitation spectrum with the Brueckner theory. For details of the simulation algorithm we refer to previous literature.^{28,29}

One way to extract the critical point is from the size dependence of the $T = 0$ spin stiffness ρ_s . Imposing a uniform twist ϕ such that the spin-spin interaction is modified according to

$$S_{ai}^x S_{aj}^x + S_{ai}^y S_{aj}^y \rightarrow (S_{ai}^x S_{aj}^x + S_{ai}^y S_{aj}^y) \cos(\phi) + (S_{ai}^y S_{aj}^x - S_{ai}^x S_{aj}^y) \sin(\phi) \quad (36)$$

(for all nearest-neighbor spin pairs in either the x or y lattice direction in both layers $a = 1, 2$) the stiffness is given by

$$\rho_s = \frac{\partial^2 E(\phi)}{\partial^2 \phi}, \quad (37)$$

where $E(\phi)$ is the internal energy per spin. The stiffness can be related to the fluctuation of the “winding number” in the Monte Carlo simulations²⁸ and can hence be evaluated directly without actually including the twist.

We study quadratic lattices with linear size L , i.e., the total number of spins is $2L^2$. According to scaling theory,³¹ at the critical point ρ_s should depend on the system size according to

$$\rho_s(q = g_c) \sim L^{d-2-z}, \quad (38)$$

where d is the dimensionality and z is the dynamic exponent. Hence, with $z = 1$, as follows if the transition is in the universality class of the 3D classical Heisenberg model, $L\rho_s$ graphed versus g for different system sizes should intersect at g_c . In Figure 3 we show results for L up to 20, calculated at temperatures sufficiently low to give the ground state (for the largest system, $L = 20$, $J/T = 320$ was used). For the largest lattices, the curves intersect at $g \approx 2.525$, in good agreement with the previous Monte Carlo estimate $g_c = 2.51 \pm 0.02^4$

Other useful quantities that can be calculated in the simulations include the static structure factors $S^\pm(\mathbf{q})$ and susceptibilities $\chi^\pm(\mathbf{q})$, which are defined according to

$$S^\pm(\mathbf{q}) = \frac{1}{2L^2} \sum_{\mathbf{r}_1, \mathbf{r}_2} e^{i\mathbf{q}\cdot(\mathbf{r}_2 - \mathbf{r}_1)} [S_{1,r_1} \pm S_{2,r_1}] [S_{1,r_2} \pm S_{2,r_2}] \quad (39a)$$

$$\chi^\pm(\mathbf{q}) = \frac{1}{2L^2} \sum_{\mathbf{r}_1, \mathbf{r}_2} e^{i\mathbf{q}\cdot(\mathbf{r}_2 - \mathbf{r}_1)} \int_0^\beta d\tau [S_{1,r_1}(\tau) \pm S_{2,r_1}(\tau)] [S_{1,r_2}(0) \pm S_{2,r_2}(0)]. \quad (39b)$$

We first consider the uniform magnetic susceptibility, $\chi = \chi^+(0, 0)$, close to the estimated g_c . According to calculations for the nonlinear σ model, $\chi(T)$ should be linear in T in the quantum critical regime, with intercept 0 at $g = g_c$. In order to study the behavior at low temperatures, lattices sufficiently large to eliminate finite-size effects have to be used. In Figure 4 we graph results at $g = 2.53$ for several system sizes. The results show that in order to obtain results reflecting the thermodynamic limit down to $T/J = 0.1$, systems with $L = 64 - 128$ are required. Note that the asymptotic $T \rightarrow 0$ behavior for a finite lattice is always an exponential decay to zero, reflecting the finite-size singlet-triplet gap (which scales to zero with increasing L for $g \leq g_c$ and remains finite for $g > g_c$). However, in the temperature regime shown in Fig. 4, the finite-size effects actually enhance χ .

In Figure 5 we show results for system sizes sufficiently large to eliminate finite-size effects for $g = 2.52$ and $g = 2.53$. For both couplings, the behavior is very close to linear for $0.1 \leq T/J \lesssim 0.4$. The intercept of a line fitted to $L = 128$ data for $T/J \leq 0.17$ is positive for $g = 2.52$ and negative for $g = 2.53$, in consistency with $g_c \approx 2.525$ estimated from the $T = 0$ stiffness scaling. Using the data shown in Fig. 5 we estimate $g_c \approx 2.525 \pm 0.002$. This result is slightly lower than estimates ($g_c = 2.54 - 2.56$) from dimer series expansions.^{3,5}

In Sec. IV we will make use of sum rules and the ratio

$$R^\pm(\mathbf{q}) = \frac{S^\pm(\mathbf{q})}{T\chi^\pm(\mathbf{q})} \quad (40)$$

to extract the approximate finite-temperature triplet excitation spectrum. Here, in Figure 6, we show the finite-size effects in $R^-(\pi, \pi)$ for $g = 2.52$ and 2.53 . The classical value of $R^\pm(\mathbf{q}) = 1$ for any \mathbf{q} , and this is also expected to hold for $R^-(\pi, \pi)$ of an antiferromagnet in the renormalized classical regime (where both the staggered structure factor and the staggered susceptibility diverge). For a system with a gap, on the other hand, both $S^\pm(\mathbf{q})$ and $\chi^\pm(\mathbf{q})$ converge to finite values for all \mathbf{q} and $R^-(\pi, \pi)$ therefore diverges as $1/T$ at low temperature. Nonlinear σ -model calculations have predicted a temperature independent $R^-(\pi, \pi)$ in the quantum critical regime, with the value $R^-(\pi, \pi) \approx 1.09$.^{11,10} Previous Monte Carlo calculations showed a reasonable agreement with this prediction close to the critical point for $T/J \approx 0.3$.¹³ The results shown in Fig. 6 demonstrate that the ratio is very sensitive to the system size at lower temperatures. The finite singlet-triplet gap present

for any finite L causes a $1/T$ behavior of R as $T \rightarrow 0$, starting at a temperature that decreases with increasing L . The results shown in Fig. 6 indicate that $L = 128$ should be sufficiently large to eliminate finite-size effects for all $T/J \geq 0.1$. For this lattice size, the data for $g = 2.52$ decreases with decreasing T whereas there is an increase for $g = 2.53$. This behavior is consistent with the predicted temperature independence exactly at g_c and $g_c \approx 2.525$. In Sec. IV we will present analytical results for the temperature corrections to $R^-(\pi, \pi)$ and make further comparisons with numerical results.

IV. RESULTS

We now discuss finite-temperature calculations at the critical point and in the quantum disordered regime. Results of the low-density Brueckner theory will be compared with quantum Monte Carlo in the $g \geq g_c$ region. Note that the critical point resulting from the self-consistent solution of the low-density Brueckner equations at zero temperature, $g_c \approx 2.320$ (see Figure 2), is different from the actual value $g_c \approx 2.525$. Unless stated otherwise, we will consider numerical results at g_c as the average of data for $g = 2.52$ and 2.53 , which should be close to the actual $g_c \approx 2.525$ critical behavior in the temperature regime considered. We compare the results with the Brueckner theory predictions for the critical point in that approach; $g = 2.320$. To compare our analytical and numerical results in the quantum disordered regime we will take $g = 3.0$ (where the Brueckner theory predictions are in perfect agreement with the numerical data at zero temperature) both for the Brueckner and Monte Carlo calculations.

A. Triplet gap

Let us first consider the critical behavior of the triplet gap, $\Delta_T = \omega_{k=0}$, described by the Brueckner equations. The temperature and the deviation from the critical point must satisfy the condition $T/J, \delta g \ll g_c$. No restriction is imposed on the ratio $\delta g/T$, however.

Close to the critical point and for small momenta ($k \ll 1$) the dispersion can be represented as

$$\omega_k \approx \sqrt{\Delta_T^2 + \gamma^2 k^2}, \quad (41)$$

where $\gamma = 1.9J$ is the zero temperature spin-wave velocity.^{5,18,32} Eq. (17) at the point $k = 0$ gives

$$\Delta_T^2 = Z_0(\tilde{A}_0^2 - \tilde{B}_0^2). \quad (42)$$

It is convenient to introduce the values of \tilde{A}_0, \tilde{B}_0 , and Z_0 at zero temperature $\tilde{A}_{T=0}, \tilde{B}_{T=0}, Z_{T=0}$, which satisfy $\Delta_0^2 = Z_{T=0}(\tilde{A}_{T=0}^2 - \tilde{B}_{T=0}^2)$. Let us vary the temperature, keeping J_\perp and J fixed. The main contribution to the variations of the integrals in Eqs. (30) and (31) comes from small momenta; $q \sim \Delta/\gamma \ll 1$. Then we find the variations of \tilde{A}_k, \tilde{B}_k at $k = 0$ to leading order:

$$\tilde{A}_0 = \tilde{A}_{T=0} + \delta\Sigma^T(0,0) - \frac{JA_cZ_c}{\pi\gamma^2}R(T) \quad (43a)$$

$$\tilde{B}_0 = \tilde{B}_{T=0} + \frac{JA_cZ_c}{\pi\gamma^2}R(T), \quad (43b)$$

where

$$\delta\Sigma^T(0,0) \approx \frac{\Gamma_c A_c Z_c}{\pi\gamma^2}R(T), \quad (44)$$

and

$$R(T) = -\Delta_T + \Delta_0 + 2T \int_{\frac{\Delta_T}{T}}^{\infty} \frac{dx_1}{e^{x_1} - 1}, \quad (45)$$

and where Γ_c , Z_c and A_c denote the vertex $\Gamma(0,0)$, the quasiparticle residue $Z_{k=0}$, and \tilde{A}_0 evaluated at $T = 0$ and $g = g_c$.

If we substitute (43) into (42) and neglect terms quadratic in Δ_T, Δ_0 , we find that the variation of the self-energy has to vanish; $\delta\Sigma^T(0,0) = 0$. Thus $R(T) = 0$ determines the finite-temperature gap Δ_T as a function of the zero temperature gap Δ_0 :

$$\frac{\Delta_T}{T} \approx \frac{\Delta_0}{T} + 2 \int_{\frac{\Delta_T}{T}}^{\infty} \frac{dx}{e^x - 1}. \quad (46)$$

Also, we have found that

$$\delta\rho^T \approx \frac{3A_c J}{4\pi\gamma^2}R(T) = 0. \quad (47)$$

Thus, as the temperature increases the quantum fluctuations are reduced while the temperature fluctuations are enhanced, the total triplet density remaining constant. After a simple integration of (46) we obtain the analytical solution

$$\Delta_T = Ty(x), \quad (48)$$

where

$$y(x) = 2\ln \left[\frac{e^{x/2}}{2} + \sqrt{1 + \frac{e^x}{4}} \right] = 2\text{arcsch} \left[\frac{1}{2}e^{x/2} \right], \quad (49)$$

with $x = \Delta_0/T$. The variable x determines whether the antiferromagnet is in the quantum critical ($x \rightarrow 0$), quantum disordered ($x \rightarrow \infty$), or the renormalized classical ($x \rightarrow -\infty$) region. It corresponds to the variables $x_1 = -2/x$ and $x_2 = 1/x$ introduced within the non-linear σ model formalism¹¹ for the critical regions in the $T - g$ plane. The zero temperature gap, $\Delta_0/J = a(g - g_c)$, is defined for positive values ($g > g_c$) but we analytically continue it to negative values ($g < g_c$). The temperature gap Δ_T depends on the coupling g via the zero temperature gap $\Delta_0(g)$. Thus, in order to calculate $\Delta_T(g)$ one should substitute Eq. (23) into (48).

The universal function $y(x)$ for the inverse correlation length, $1/\xi = \Delta_T$, is exactly the same as that previously obtained for the nonlinear σ model ($N \rightarrow \infty$),¹¹ with the limiting behavior

$$y(x) = 2\ln\frac{1+\sqrt{5}}{2} + \frac{x}{\sqrt{5}}, \quad x \rightarrow 0, \quad (50a)$$

$$y(x) \approx x + 2e^{-x}, \quad x \rightarrow \infty, \quad (50b)$$

$$y(x) \approx e^{x/2}, \quad x \rightarrow -\infty. \quad (50c)$$

Thus the correlation length is exponentially large in the renormalized classical region, proportional to $1/T$ in the quantum-critical region, and of the order $1/\Delta_0$ in the quantum disordered regime. At the critical point ($x = 0$) we have

$$\Delta_T = y_0 T, \quad y_0 = 2\ln\left[\frac{1+\sqrt{5}}{2}\right] \approx 0.962424. \quad (51)$$

In Figure 7 we compare the analytical result (48) at $g = g_c$, and $g = 3.0$ obtained under the assumption of small T and δg with the corresponding self-consistent numerical solutions of the Brueckner equations for the triplet gap. The agreement is very good for $g = g_c$ at low temperatures, and slightly worse at $g = 3.0$.

Now, let us consider the following dimensionless ratio

$$R(\mathbf{q}) = \frac{S(\mathbf{q})}{T\chi(\mathbf{q})}, \quad (52)$$

where $S(\mathbf{q})$, $\chi(\mathbf{q})$ are the odd (-) static structure factor and susceptibility defined in Eqs. (39) [with the momentum shifted by (π, π)]. They are related to the corresponding dynamic structure factor,

$$S(\mathbf{q}, \omega) = \text{Im} \int e^{i\omega t} \langle T(\mathbf{S}(\mathbf{q}, t)\mathbf{S}(-\mathbf{q}, 0)) \rangle dt, \quad (53)$$

where $\mathbf{S}_i = \mathbf{S}_{1i} - \mathbf{S}_{2i}$, via the sum rules³³

$$S(\mathbf{q}) = \frac{1}{\pi} \int_0^\infty S(\mathbf{q}, \omega) (1 + e^{-\omega/T}) d\omega, \quad (54a)$$

$$\chi(\mathbf{q}) = \frac{2}{\pi} \int_0^\infty S(\mathbf{q}, \omega) (1 - e^{-\omega/T}) \frac{d\omega}{\omega}. \quad (54b)$$

Taking into account the contribution from the elementary triplet only, the structure factor can be written in the form

$$S(q, \omega) = (u_{\mathbf{q}} + v_{\mathbf{q}})^2 \delta(\omega - \omega_{\mathbf{q}}). \quad (55)$$

Then, using the above sum rules (54a) and (54b), the dimensionless ratio $R(\mathbf{q})$ can be rewritten in the form

$$R(\mathbf{q}) = \frac{1 + e^{-\omega_{\mathbf{q}}/T}}{1 - e^{-\omega_{\mathbf{q}}/T}} \frac{\omega_{\mathbf{q}}}{2T}. \quad (56)$$

The importance of this ratio is that it can be obtained using Monte Carlo simulations by calculating the static susceptibility and structure factor, as discussed in Sec. III. The spectrum of elementary excitations, $\omega_{\mathbf{q}}$, can then be extracted from Eq. (56). At zero momentum, $q = 0$, the critical behavior of $R(0)$ is given by

$$R(0) = \frac{y(x)}{2} \frac{1 + e^{-y(x)}}{1 - e^{-y(x)}}. \quad (57)$$

Then the limiting behavior of $R(0)$ is readily obtained from Eq. (48):

$$R(0) = \frac{\sqrt{5}}{2} \left(y_0 + \frac{x}{\sqrt{5}} \left(1 - \frac{2}{\sqrt{5}} y_0 \right) \right), \quad x \rightarrow 0, \quad (58a)$$

$$R(0) = \frac{x}{2} + e^{-x}(1 + x), \quad x \rightarrow \infty, \quad (58b)$$

$$R(0) = 1 - \frac{e^{x/2}}{2}, \quad x \rightarrow -\infty. \quad (58c)$$

We have calculated $R(0)$ as a function of temperature using quantum Monte Carlo simulations close to the critical point, at $g = 2.52$ and 2.53 , and using the Brueckner equations at the critical point ($x = 0$). As discussed in Sec. III (Fig. 4), $R(0)$ is very sensitive to the lattice size at low temperatures. In Figure 8 we show Monte Carlo results for systems sufficiently large to eliminate finite-size effects (linear size L up to 128). In Sec. III the critical point was determined to be $g_c = 2.525 \pm 0.002$. Even for $|g - g_c|$ as small as 0.005, there are very large differences between the $g - g_c > 0$ and $g - g_c < 0$ data. In order to extract the behavior exactly at $g = g_c$, simulations would have to be carried out for values of g also between 2.52 and 2.53, and the critical point would have to be determined to even higher accuracy. The available data nevertheless shows that the Brueckner theory is very accurate. The analytical curve falls between the two numerical data sets at low temperature, and the T dependence at high temperatures is also very well reproduced. In the Brueckner theory $R(0) \rightarrow 1.076$ at $g \rightarrow g_c$ as $T \rightarrow 0$. The numerical results suggest that the exact value is slightly higher, but close to 1.08.

The temperature dependent triplet gap extracted from the Monte Carlo data for $R(0)$ using Eq. (56) is presented in Figure 7, along with our analytical prediction. The agreement is almost perfect at the critical point, while at $g = 3.0$ it is not so good but still quite reasonable.

The formula (56) is not exact, due to the neglected contribution of the three-particle continuum and broadening. Note that the contribution of the two-particle continuum is canceled by symmetry. The three-particle continuum is negligible only near the $q = (0, 0)$ at the critical point while it can be important in other cases.

Using Eq. (56), we can extract the triplet spectrum $\omega_{\mathbf{k}}$ from the Monte Carlo results for $R(\mathbf{q})$. In Figure 9 we compare it with the solution of the Brueckner equations at $g = g_c$ and $T = 0.5J$. The agreement between the Monte Carlo and analytical results is even better than might be expected (the agreement remains very good also at lower temperatures). The Brueckner approximation should be accurate if the triplet density ρ is low, but in fact it is as high as $\rho \sim 0.1$.¹⁸ The surprisingly good agreement justifies Eq. (56) and the assumption that the dynamic structure factor is peaked at $\omega = \omega_{\mathbf{k}}$ [see Eq. (55)]. Thus the broadening is negligible and the elementary triplet is well defined for $g \geq g_c$ at low temperature. However, the broadening can be important for $g < g_c$.

B. Specific heat

The calculation of the specific heat, C_V , is straightforward. The energy of the system cannot be written as a simple summation over quasiparticle energies, $E \neq \sum \omega_k n_k$, due to the strong interaction. However, one can write the energy variation as $\delta E = \sum \omega_k \delta n_k$, in analogy with the Landau theory of Fermi liquids. Thus, the specific heat per spin is

$$C_V = \frac{3}{2L^2} \sum_{\mathbf{k}} \omega_{\mathbf{k}} \frac{\partial n_{\mathbf{k}}}{\partial T}. \quad (59)$$

It is convenient to use Eq. (59) instead of taking of the second derivative, $C_V = -\frac{1}{2}T\partial^2 F/\partial T^2$, using Eq. (34). The specific heat calculated from Eq. (59) and the self-consistent solution of the Brueckner equations is shown in Figure 10 as a function of T at $g = g_c$ and $g = 3.0$. We have also calculated the specific heat by fitting a high-order polynomial to the internal energy obtained using quantum Monte Carlo simulations. As seen in Fig. 10, the agreement between the analytical and numerical results is excellent for $T < 0.5J$. The agreement is perfect at the critical point, while at $g = 3.0$ it is not so good. The reason for this can be traced to the fact that the value of triplet gap, $\Delta_0 \approx 0.78J$, at $T = 0, g = 3.0$ in our analytic method is slightly different from the numerical result $\Delta_0 \approx 0.75J$ at zero temperature. This difference leads to a slightly different exponent for the specific heat.

In the limit $T \ll J, g \rightarrow g_c$, the expression for the specific heat can be found explicitly by combining Eqs. (41), (48) and (59):

$$C_V = \frac{3\zeta(3)T^2}{2\pi\gamma^2} \Psi\left(\frac{\Delta_0}{T}\right), \quad (60)$$

where the universal function Ψ is given by

$$\Psi(x) = \frac{1}{2\zeta(3)} \int_{y(x)}^{\infty} \frac{dx_1 x_1 e^{x_1}}{(e^{x_1} - 1)^2} \left[x_1^2 - y^2(x) + xy(x) \frac{dy(x)}{dx} \right]. \quad (61)$$

The coefficient of $\Psi(x)$ in (60) has been chosen to be the specific heat of a single gapless Bose degree of freedom with dispersion $\omega = \gamma k$ in two dimensions. The value of $\Psi(x)$ at $T \rightarrow 0$ is thus a measure of the effective number of such modes in the ground state. In the renormalized classical limit, it has the value $\Psi(-\infty) = 3$, while at the critical point $\Psi(0) = \frac{4}{5}\Psi(-\infty)$. In the quantum disordered limit, $x \rightarrow \infty$, we find exponentially small specific heat:

$$C_V \approx \frac{3T^2}{4\pi\gamma^2} x^3 e^{-x}, \quad x \rightarrow \infty.$$

Thus $\Psi(\infty) = 0$, corresponding to the absence of any gapless degrees of freedom. The limiting behavior of universal function $\Psi(x)$ is exactly the same as obtained one for the nonlinear σ -model ($N \rightarrow \infty$).¹¹

The fact that $\Psi(-\infty) = 3$ implies that our approach does not describe well the physics for $g < g_c$, where the spin dynamics is well described by rotationally averaged spin-wave (Goldstone) fluctuations about a Neel-ordered ground state. There are only two gapless modes in the renormalized classical regime, while in our approach there are three, and the critical and Goldstone fluctuations are indistinguishable. The application of the Brueckner theory in this phase requires modifications; a nonzero sublattice magnetization, i.e., a single particle condensate at zero momentum, has to be introduced.

C. Uniform magnetic susceptibility

Let us now calculate another important physical observable — the magnetic susceptibility. If a uniform magnetic field of strength \mathbf{h} is applied, then the term

$$H_h = -\mathbf{h} \cdot \sum_i \mathbf{S}_i = ih_\alpha e_{\alpha\beta\gamma} \sum_{\mathbf{k}} t_{\mathbf{k}\beta}^\dagger t_{\mathbf{k}\gamma}, \quad (62)$$

should be added to the Hamiltonian (3).

Let us first to concentrate on the zero temperature properties. The second order correction to the total energy of the system due to the perturbation (62) is given by the diagrams shown, in Figure 11(a),

$$E^{(2)} \sim h^2 \sum_{\mathbf{k}} \int \frac{d\omega}{2\pi} [G_n(\mathbf{k}, \omega) G_n(\mathbf{k}, \omega) - G_a(\mathbf{k}, \omega) G_a(\mathbf{k}, \omega)]. \quad (63)$$

where $G_n(\mathbf{k}, t) = -i \langle T(t_{\mathbf{k}\alpha}(t) t_{\mathbf{k}\alpha}^\dagger(0)) \rangle$ and $G_a(\mathbf{k}, t) = -i \langle T(t_{-\mathbf{k}\alpha}^\dagger(t) t_{\mathbf{k}\alpha}^\dagger(0)) \rangle$ are normal and anomalous Green's functions at zero temperature which can be formally obtained by setting $n_{\mathbf{k}} \equiv 0$ in the expressions (27) and (28). After a simple integration over ω , one can show that $E^{(2)} = 0$. Thus, the uniform magnetic susceptibility per spin,

$$\chi = -\frac{1}{2} \frac{\partial^2 \mathbf{F}}{\partial h^2} \Big|_{h=0}, \quad (64)$$

is zero at $T = 0$. It is worth noting that the Bogoliubov transformation (6) does not change the operator of the magnetic moment $M_\alpha = -ie_{\alpha\beta\gamma} \sum_{\mathbf{k}} t_{\mathbf{k}\beta}^\dagger t_{\mathbf{k}\gamma} = -ie_{\alpha\beta\gamma} \sum_{\mathbf{k}} a_{\mathbf{k}\beta}^\dagger a_{\mathbf{k}\gamma}$.

To calculate the uniform susceptibility at finite temperature, let us demonstrate that within the framework of the Brueckner approach the perturbation (62) splits a three degenerate triplet into excitations at ω_k and $\omega_k \pm \mu \cdot h$ with magnetic moment $\mu = 1$ at zero temperature. The correction to the self-energy due to the magnetic field \mathbf{h} is given by the diagrams (b) and (c) in Figure 11:

$$\begin{aligned} \delta\Sigma_{\beta\gamma}^h(\mathbf{K}) &= ih_\alpha e_{\alpha\beta\gamma} \left(1 - i \int \Gamma(\mathbf{K} + \mathbf{Q}) [G_n(\mathbf{Q}) G_n(\mathbf{Q}) - G_a(\mathbf{Q}) G_a(\mathbf{Q})] \frac{d^3 \mathbf{Q}}{(2\pi)^3} - \right. \\ &\quad \left. - 5 \int \Gamma^2(\mathbf{K} + \mathbf{Q}) G_n(\mathbf{K} + \mathbf{Q} - \mathbf{Q}_1) G_n^2(\mathbf{Q}_1) G_n(\mathbf{Q}) \frac{d^3 \mathbf{Q}_1}{(2\pi)^3} \frac{d^3 \mathbf{Q}}{(2\pi)^3} \right) = \\ &= ih_\alpha e_{\alpha\beta\gamma} \left[1 - \frac{\partial \Sigma^{h=0}}{\partial \omega} \Big|_{\omega=0} \right] = ih_\alpha e_{\alpha\beta\gamma} Z_{\mathbf{k}}^{-1}. \end{aligned} \quad (65)$$

The first diagram in Fig. 11(b) results in a trivial correction, $ih_\alpha e_{\alpha\beta\gamma}$, the second and the third diagrams [the term linear in $\Gamma(K)$ in eq.(65)] give $(i/4)h_\alpha e_{\alpha\beta\gamma} \partial \Sigma / \partial \omega$, and the diagrams in Fig. 11(c) [the term quadratic in $\Gamma(K)$ in the eq.(65)] yield $-(5/4)ih_\alpha e_{\alpha\beta\gamma} \partial \Sigma / \partial \omega$. Further separation of a quasiparticle contribution in a Green's function for physical operators $a_{\mathbf{k}\alpha}$ with polarization α taken in spiral coordinates,

$$\frac{1}{\omega - \tilde{\omega}_{\mathbf{k}} - \Sigma(\mathbf{k}, \omega) + \varepsilon \cdot h \cdot Z_{\mathbf{k}}} \approx \frac{Z_{\mathbf{k}}}{\omega - \omega_{\mathbf{k}} + \varepsilon \cdot h},$$

with $\varepsilon = -1, 0, 1$, results in a simple Zeeman splitting of the elementary triplet excitation. Thus, instead of three degenerate triplets at $\omega_{\mathbf{k}}$ there are three excitations at $\omega_{\mathbf{k}}$ and $\omega_{\mathbf{k}} \pm h$, i.e., for magnetic moment $\mu = 1$. We can now calculate the magnetic susceptibility at finite temperature. Since the temperature correction to the renormalization constant is a very small, the main temperature correction to the self-energy is due to the second and third diagrams in Fig. 11(b). We use the conventional Matsubara technique ($\omega \rightarrow i\omega_n$) to calculate this correction and obtain

$$\delta\Sigma^{T,h} = -ih_\alpha e_{\alpha\beta\gamma} \frac{\Gamma(p, 0)}{4TL^2} \sum_{\mathbf{q}} \frac{1}{\sinh^2(\omega_{\mathbf{q}}/2T)}. \quad (66)$$

Using (65) and (66) one can find the quasiparticle magnetic moment renormalized due to temperature:

$$\mu(\mathbf{p}) = 1 - \frac{Z_{\mathbf{p}}\Gamma(\mathbf{p}, 0)}{4TL^2} \sum_{\mathbf{q}} \frac{1}{\sinh^2(\omega_{\mathbf{q}}/2T)}. \quad (67)$$

Then the uniform magnetic susceptibility per spin can be easily obtained from

$$\chi = \frac{1}{2} \frac{\partial M}{\partial h} \Big|_{h=0}, \quad M = -\frac{2}{N} \sum_{\mathbf{p}} \frac{\partial n_{\mathbf{p}}}{\partial \omega_{\mathbf{p}}} \mu(\mathbf{p}) \cdot h. \quad (68)$$

Figure 12 shows the magnetic susceptibility as a function of temperature at $g = g_c$ and at $g = 3.0$, as obtained from Eq. (68) using the self-consistent solution of the Brueckner equations. In the same figure we also show our quantum Monte Carlo results. The agreement between the both methods is excellent at low temperature. The agreement at critical point is better than at $g = 3.0$ because the value of triplet gap, $\Delta_0 \approx 0.78J$, at $T = 0, g = 3.0$ in our analytic method is slightly different from numerical result $\Delta_0 \approx 0.75$. This difference leads to a slightly different exponent for the magnetic susceptibility.

In the critical region, where $T \ll J, \delta g \ll g_c$, the main contribution to the integration in (67) is due to small momenta, $q \sim \Delta/\gamma$, thus the susceptibility per spin can be written as

$$\chi = \frac{T}{2\pi\gamma^2} \Omega(x), \quad (69)$$

with the universal function

$$\begin{aligned} \Omega(x) &= \int_{y(x)}^{\infty} \frac{dx_1 x_1 e^{x_1}}{(e^{x_1} - 1)^2} \left[1 - \delta_0 T \int_{y(x)}^{\infty} \frac{x_1 dx_1}{\sinh^2 \frac{x_1}{2}} \right] = \\ &= \frac{1}{2} \left[y(x) \operatorname{ctanh} \frac{y(x)}{2} - x \right] \left[1 - 2\delta_0 T \left(y(x) \operatorname{ctanh} \frac{y(x)}{2} - x \right) \right]. \end{aligned} \quad (70)$$

The constant $\delta_0 = Z_c \Gamma_c / (8\pi\gamma^2) \approx 0.06$ has been evaluated using the values of $\Gamma_c \approx 6.3J, Z_c \approx 0.8, \gamma \approx 1.9J$ taken from the self-consistent solution of the Brueckner equations at zero temperature, see Refs. 18,20. The universal function $\Omega(x)$ has the limiting behavior

$$\Omega(x) \approx \frac{\sqrt{5}}{2} y_0 \left(1 - \frac{2}{5}x\right) (1 - 2\delta_0 T \sqrt{5} y_0), \quad x \rightarrow 0 \quad (71)$$

$$\Omega(x) \approx -\frac{x}{2} \left(1 - \frac{2}{x}\right) (1 + 2\delta_0 \Delta_0), \quad x \rightarrow -\infty \quad (72)$$

$$\Omega(x) \approx x e^{-x} \left(1 + \frac{1}{x}\right), \quad x \rightarrow \infty, \quad (73)$$

which is exactly the same as predicted using the nonlinear σ model ($N \rightarrow \infty$)^{10,11} if corrections proportional to δ_0 are neglected. These corrections are subleading terms, but in the quantum critical and renormalized classical regimes they are parametrically larger than the subleading terms obtained for the σ model ($N \rightarrow \infty$).

V. CONCLUSIONS AND DISCUSSION

In conclusion, we have presented an effective, self-consistent diagrammatic approach to describe the properties of the quantum double-layer Heisenberg antiferromagnet at low temperature and $g \geq g_c$. To account for strong correlations between the elementary excitations (triplets), we applied the Brueckner approximation, treating the triplets as a dilute Bose gas with infinite on-site repulsion. We have also used a numerically exact quantum Monte Carlo simulation method to obtain non-perturbative results for comparison. We have calculated temperature dependent spectra (including the triplet gap), dynamic and static structure factors, the specific heat, and the uniform magnetic susceptibility. The agreement between the analytical and numerical results is excellent.

Our analytical method involves approximations and an error of a few percent is always expected. The diagrammatic approach is valid for small on-site density of excitations because we neglected anomalous contributions in the vertex $\Gamma(\mathbf{K})$. We emphasize, however, that the region of applicability of the present technique is surprisingly large. The reason for this can be traced to the fact that the density of triplets increases rather slowly as a function of temperature. We found that near the critical point: $\rho^T = 0.15$ for $T = 0.5J$ while $\rho = 0.12$ at $T = 0$. It justifies the approach even for a relatively high temperatures, $T \sim 0.5J$, when $g \geq g_c$.

The Brueckner approach allows to calculate the elementary triplet spectrum $\omega_{\mathbf{k}}$ at finite temperature, not only for small momentum but in the whole Brillouine zone. Comparing the analytical results for the dimensionless ratio $R(\mathbf{q}) = S(\mathbf{q})/T\chi(\mathbf{q})$ with quantum Monte Carlo data, we demonstrated that the dynamic structure factor is peaked at $\omega = \omega_{\mathbf{k}}$, the broadening of the triplet excitation is negligible and the elementary triplet is well defined for $g \geq g_c, T < 0.5J$.

In the $T \ll J$ and $g \rightarrow g_c$ limit, our analytical results show that correlation length, the specific heat, and the magnetic susceptibility are universal functions of the zero temperature gap, Δ_0 , the spin-wave velocity, γ , and the temperature, T . The universal functions for the specific heat and the correlation length have the same limiting behavior as those predicted using the nonlinear σ -model ($N \rightarrow \infty$), while our universal function of the magnetic susceptibility contains additional subleading terms.

The agreement with the σ model approach is due to the relative smallness of the quartic interaction, Eq. (4b), for the two-layer Heisenberg model considered in this paper. In this

situation, the hard-core constraint is the most important and it is very natural that the results correspond to that of the σ model. However, this situation is not general. There are many models where the quartic interaction is very important. It can even produce bound states of triplet spin-waves²¹ which effectively change the number of relevant degree of freedom. In this situation, one can expect a very substantial deviation from the simple nonlinear σ -model behavior, while the above Brueckner approach can still be applied. An important example of such a system is the 2D $J_1 - J_2$ model where the singlet bound state has an extremely low energy.²³

The Brueckner theory describes quite well the quantum critical and quantum disordered phases near the quantum critical point, as evidenced by the very good agreement with the quantum Monte Carlo results. However, the description of the renormalized classical regime is not good in this theory because the “Goldstone” regime with a Josephson length scale ξ_J , where the spin dynamics is well described by rotationally averaged spin-wave fluctuations about a Neel-ordered ground state, is not present in our approach. In the Brueckner approach the critical and Goldstone fluctuations are indistinguishable. It is well known, however, that there are only two gapless modes in the renormalized classical regime, while in our approach there are three. The application of the Brueckner theory in this phase requires modifications; a nonzero sublattice magnetization N_z , i.e., a single particle condensate at zero momentum, has to be introduced. We plan to consider this in a future study.

The advantages of our analytic approach are that it is simple and captures the essential physics, as demonstrated here by comparing results with quantum Monte Carlo simulations as well as with predictions from the nonlinear σ model. Obvious other applications of the Brueckner method include 2D Heisenberg models with frustration, Heisenberg ladders, as well one-dimensional spin chains at finite temperature.

In addition to confirming the high accuracy of the Brueckner theory, the quantum Monte Carlo simulations performed here also show unambiguously that quantum critical behavior can be observed in the bilayer model at temperatures as high as $T/J \lesssim 0.5$. We also obtained an improved estimate of the critical coupling ratio; $g_c = 2.525 \pm 0.002$.

VI. ACKNOWLEDGMENTS

We are very grateful to V. Kotov, R. Singh, G. Gribakin and M. Kuchiev for stimulating discussions. This work was supported by a grant from the Australian Research Council. A. W. S. would like to thank the School of Physics at the University of New South Wales for hospitality and financial support during a visit. Support from the NSF under Grant No. DMR-9712765 is also acknowledged.

REFERENCES

- ¹ A. J. Millis and H. Monien, Phys. Rev. Lett. **70**, 2810 (1993).
- ² A. J. Millis and H. Monien, Phys. Rev. B **50**, 16606 (1994).
- ³ K. Hida, J. Phys. Soc. Jpn. **59**, 2230 (1990).
- ⁴ A. W. Sandvik and D. J. Scalapino, Phys. Rev. Lett. **72** 2777 (1994).
- ⁵ Z. Weihong, Phys. Rev. B **55**, 12267 (1997).
- ⁶ D. Reznik *et al.*, Phys. Rev. B **54**, 14741 (1996); S. M. Hayden *et al.*, Phys. Rev. B **54**, 6905 (1996).
- ⁷ For a review see, S. Sachdev, in *Low Dimensional Quantum Field Theories for Condensed Matter Physicists*, edited by L. Yu, S. Lundqvist and G. Morlandi, World Scientific (1995).
- ⁸ F. D. M. Haldane, Phys. Rev. Lett. **50**, 1153 (1983)
- ⁹ S. Chakravarty, B. I. Halperin, and D. R. Nelson, Phys. Rev. Lett. **60**, 1057 (1988); Phys. Rev. B **39**, 2344 (1989).
- ¹⁰ S. Sachdev, J. Ye, Phys. Rev. Lett **69**, 2411 (1992).
- ¹¹ A. V. Chubukov, S. Sachdev, and J. Ye, Phys. Rev. B **49**, 11919 (1994).
- ¹² A. W. Sandvik and M. Vekić, J. Low. Temp. Phys. **99**, 367 (1995).
- ¹³ A. W. Sandvik, A. V. Chubukov and S. Sachdev, Phys.Rev.B **51** 16483 (1995).
- ¹⁴ J. Oitmaa, R. R. P. Singh, and W. H. Zheng, Phys. Rev. B **54**, 1009 (1996).
- ¹⁵ J. Jaklic and P. Prelovsek, Phys. Rev. Lett. **77**, 892 (1996).
- ¹⁶ N. Elstner and R. R. P. Singh, Phys. Rev B **57**, 7740 (1998).
- ¹⁷ A. V. Chubukov and D. Morr, Phys. Rev. B **54**, 3468 (1996).
- ¹⁸ V. N. Kotov, O. Sushkov, Z. Weihong and J. Oitmaa, Phys. Rev. Lett. **80**, 5790 (1998).
- ¹⁹ See, e.g., A. L. Fetter and J. D. Walecka, *Quantum Theory of Many Particle Systems*, McGraw-Hill, New York, 1971
- ²⁰ P. V. Shevchenko and O. P. Sushkov, cond-mat/9809368, to appear in Phys. Rev. B **59** (1999).
- ²¹ O. P. Sushkov and V. N. Kotov, Phys. Rev. Lett. **81**, 1941 (1998).
- ²² P. V. Shevchenko, V. N. Kotov and O. P. Sushkov, cond-mat/9901302.
- ²³ V. N. Kotov, J. Oitmaa, O. P. Sushkov and Z. Weihong, cond-mat/9903154.
- ²⁴ A. V. Chubukov, JETP Lett, bf 49, 129 (1989).
- ²⁵ S. Sachdev and R. Batt, Phys. Rev. B **41**, 9323 (1990).
- ²⁶ A. A. Abrikosov, L. P. Gorkov, and I. E. Dzyaloshinski, "Methods of Quantum Field Theory in Statistical Physics", Dover (1975).
- ²⁷ A. W. Sandvik and J. Kurkijärvi, Phys. Rev. B **43**, 5950 (1991); A. W. Sandvik, J. Phys. A **25**, 3667 (1992).
- ²⁸ A. W. Sandvik, Phys. Rev. B **56**, 11678 (1997).
- ²⁹ A. W. Sandvik, cond-mat/9902226 (to appear in Phys. Rev. B, June 1999).
- ³⁰ H. G. Evertz, G. Lana, and M. Marcu, Phys. Rev. Lett. **70**, 875 (1993); N. Kawashima, J. E. Gubernatis, and H. Evertz, Phys. Rev. B **50**, 136 (1994); B. B. Beard and U. -J Wiese, Phys. Rev. Lett. **77**, 5130 (1996).
- ³¹ M. Wallin, E. S. Sørensen, S. M. Girvin, and A. P. Young, Phys. Rev. B **49**, 12115 (1994).
- ³² K. Hida, J. Phys. Soc. Jpn. **61**, 1013 (1992); M. P. Gelfand, Phys. Rev. B **53**, 11309 (1996).
- ³³ P. C. Hohenberg, W. F. Brinkman, Phys. Rev. B **10**, 128 (1974)

FIGURES

FIG. 1. a) Equation for the scattering vertex $\Gamma(\mathbf{K})$. b) Diagram for the self-energy $\Sigma(\mathbf{K})$ corresponding to $\Gamma(\mathbf{K})$.

FIG. 2. Triplet gap, Δ/J , as a function of coupling $g = J_{\perp}/J$. Solid and dashed lines are the results of the self-consistent solution using the Brueckner approach and the Brueckner equations linearized in density, respectively. The dots with error bars are estimates obtained by dimer series expansions.¹⁸

FIG. 3. QMC results for the $T = 0$ spin stiffness ρ_s times the linear system size L , for $L = 4, 6, \dots, 16, 20$. The curves are quadratic fits to the QMC data (solid circles). The (negative) slope of $L\rho_s$ vs g increases with L . Statistical errors are typically of the order of the radius of the circles.

FIG. 4. The uniform magnetic susceptibility, χJ , per spin vs temperature, T/J , for different system sizes at a coupling $g = 2.53$. Statistical errors are much smaller than the symbols.

FIG. 5. The uniform magnetic susceptibility, χJ , per spin vs temperature, T/J , for $g = 2.52$ and 2.53 . The lines are fits to the $T/J \leq 0.17$ data.

FIG. 6. The ratio of the staggered structure factor and T times the staggered susceptibility for $L = 32$ (solid circles), $L = 64$ (open circles), and $L = 128$ (solid squares), for a coupling slightly below ($g = 2.52$) and above ($g = 2.53$) the critical coupling as a function of temperature, T/J . Statistical errors are at most of the order of the size of the symbols. The dashed lines indicate the constant value predicted within the nonlinear σ -model approach.

FIG. 7. Deviation $\delta\Delta = (\Delta_T - \Delta_0)/J$ as a function of temperature, T/J , at the critical point, $g = g_c$, and in the quantum disordered regime at $g = 3.0$. Solid lines are results of self-consistent solutions of the Brueckner equations linearized in density, dots are estimates extracted from Monte Carlo simulations for $R(0)$ using Eq.(57), and dashed lines are predictions of the analytical Eq. (48).

FIG. 8. The dimensionless ratio $R(0) = S(0)/[T\chi(0)]$ as a function of temperature, T/J , for $g = 2.52$ and $g = 2.53$ obtained using quantum Monte Carlo simulation (dots). The solid line is the analytical result for $g = g_c$ obtained from the self-consistent solution of the Brueckner equations.

FIG. 9. Elementary triplet spectrum, $\omega(q)/J$, along the triangle in Brillouine zone, $q = (0, 0) - (\pi, \pi) - (\pi, 0) - (0, 0)$, at $g = g_c, T = 0.5J$. The solid line is the result of a self-consistent solution of the Brueckner equations, the dots are estimates extracted from Eq. (56) and Monte Carlo results for $R(q)$.

FIG. 10. Specific heat per spin, C_V , as a function of temperature T/J at critical point $g = g_c$ and $g = 3.0$. Solid lines are the results of self-consistent solution of Brueckner equations, dots are estimates obtained by Monte Carlo simulations.

FIG. 11. a) Diagrams for the second order correction to the total energy due to a magnetic field perturbation. b),c) the diagrams for the correction to the normal self energy due magnetic field.

FIG. 12. Magnetic susceptibility per spin, χJ , as a function of temperature, T/J , at $g = g_c$ and $g = 3.0$. The solid lines are results of self-consistent solutions of the Brueckner equations linearized in density. The dots are Monte Carlo results.

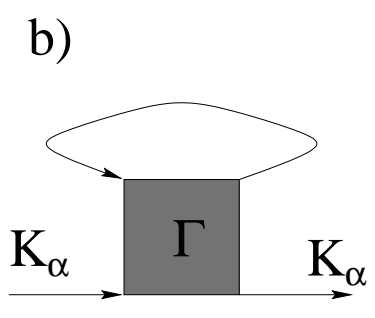
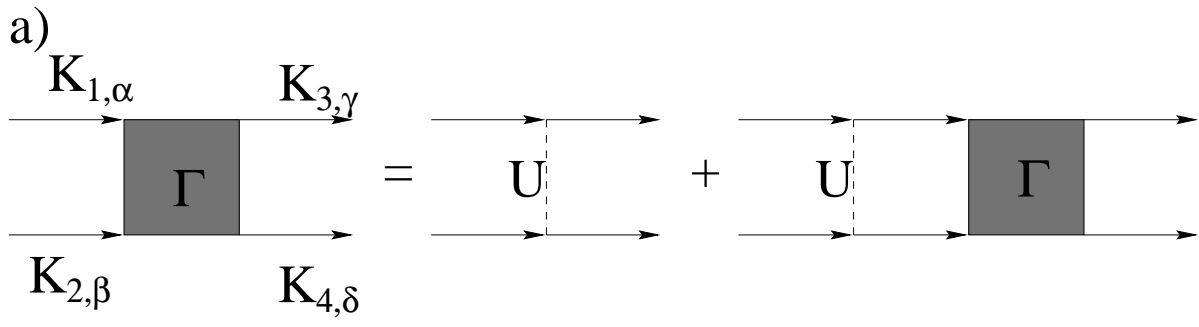


Fig.1

Fig.2

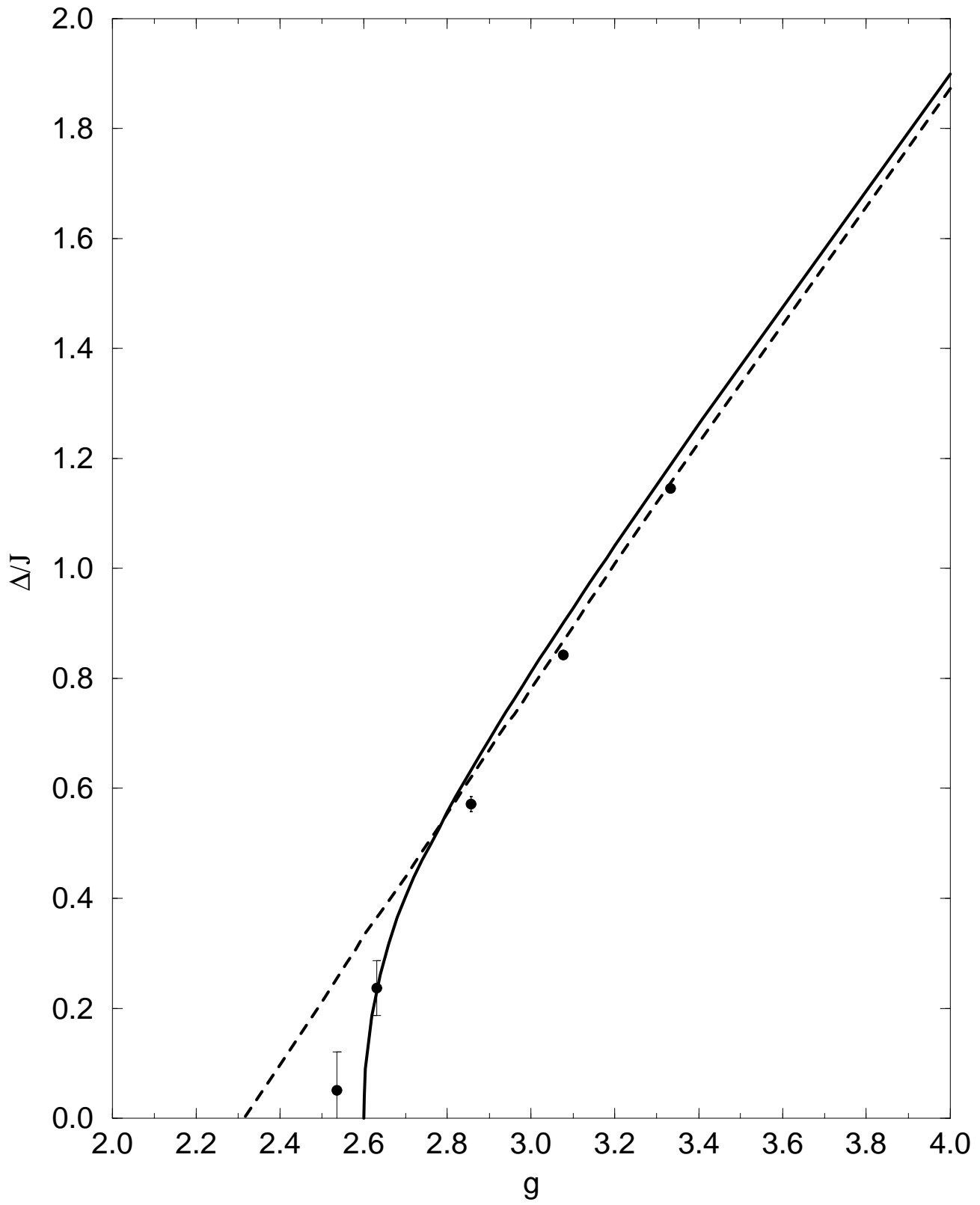


Fig.3

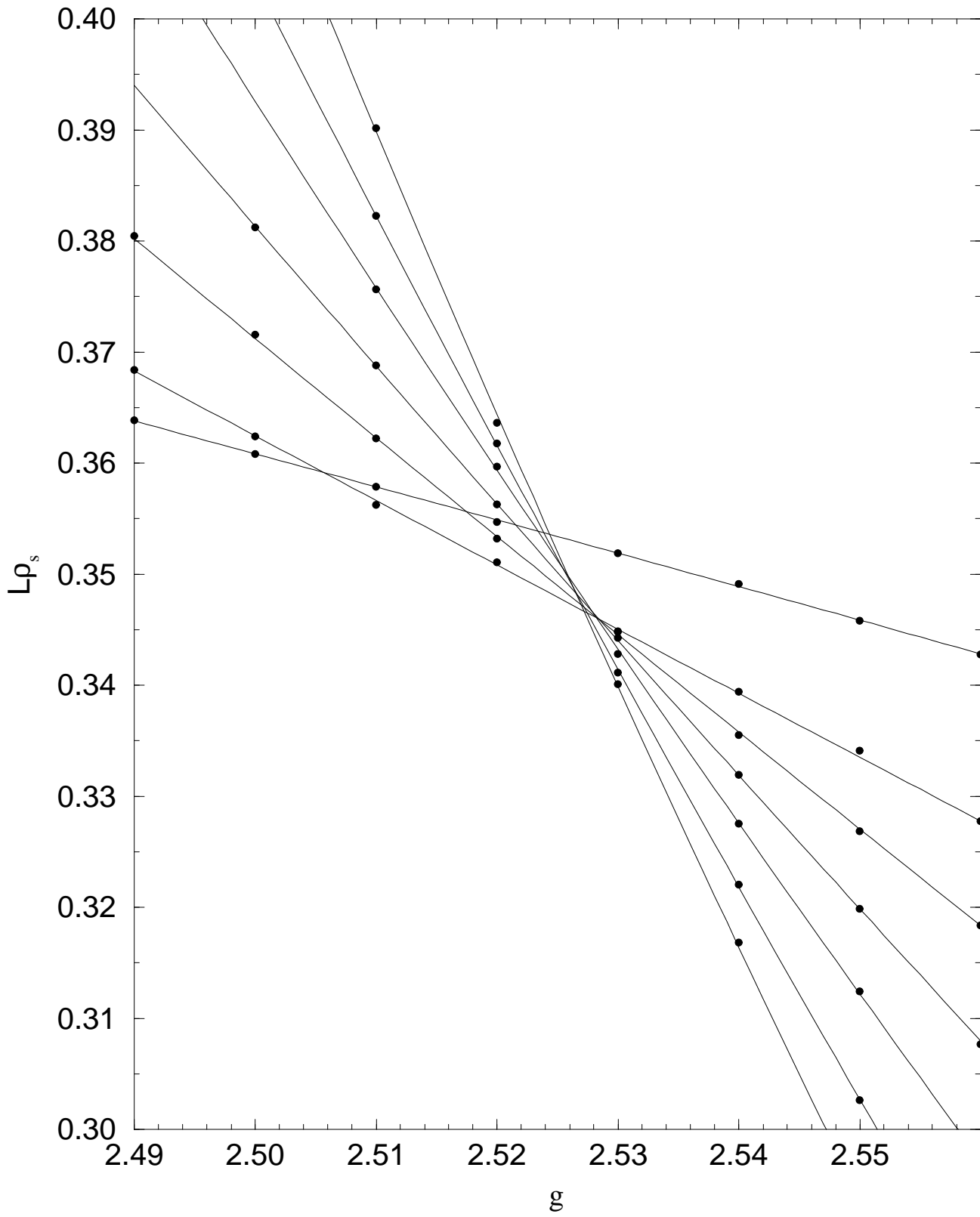


Fig.4

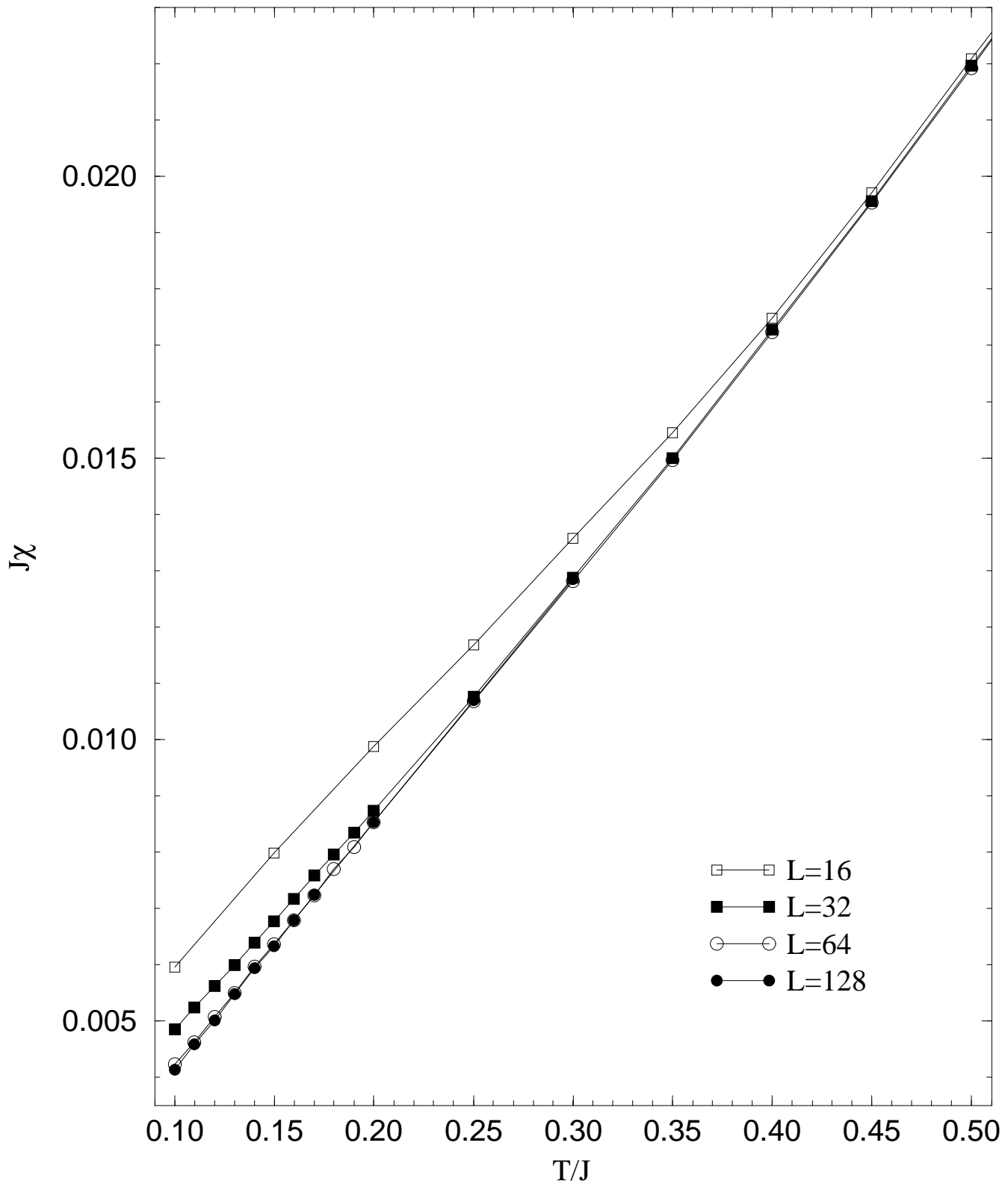


Fig.5

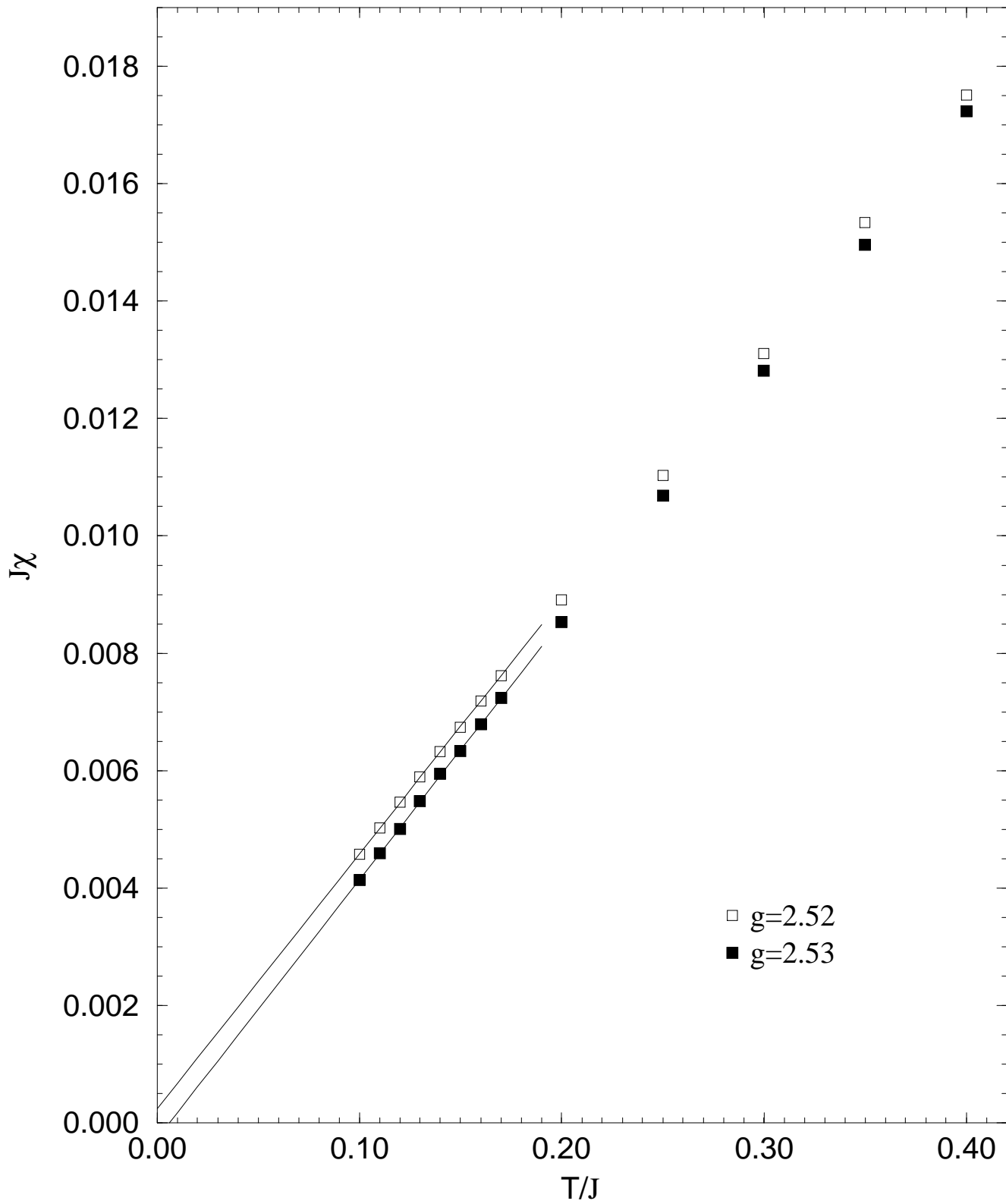


Fig.6

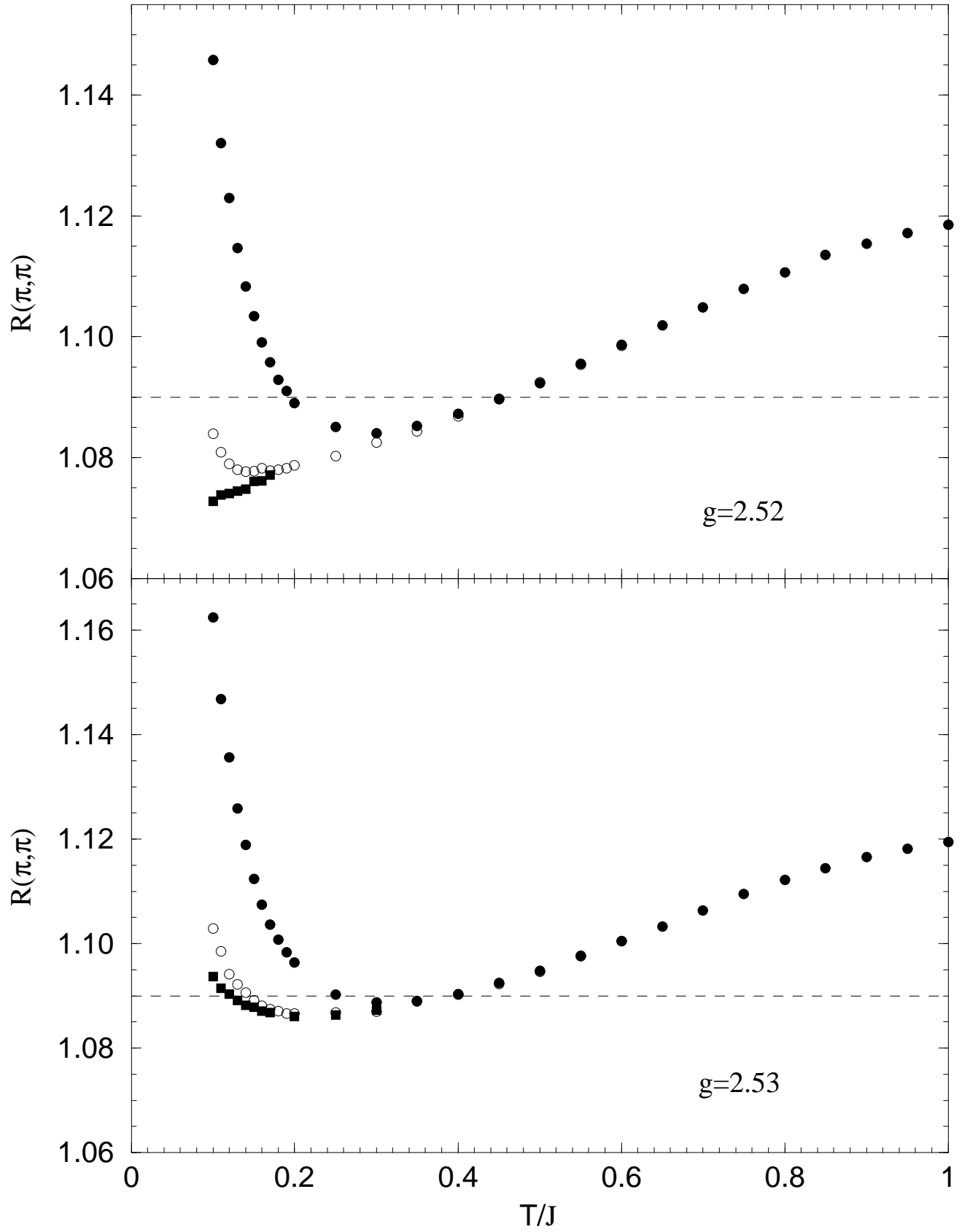


Fig.7

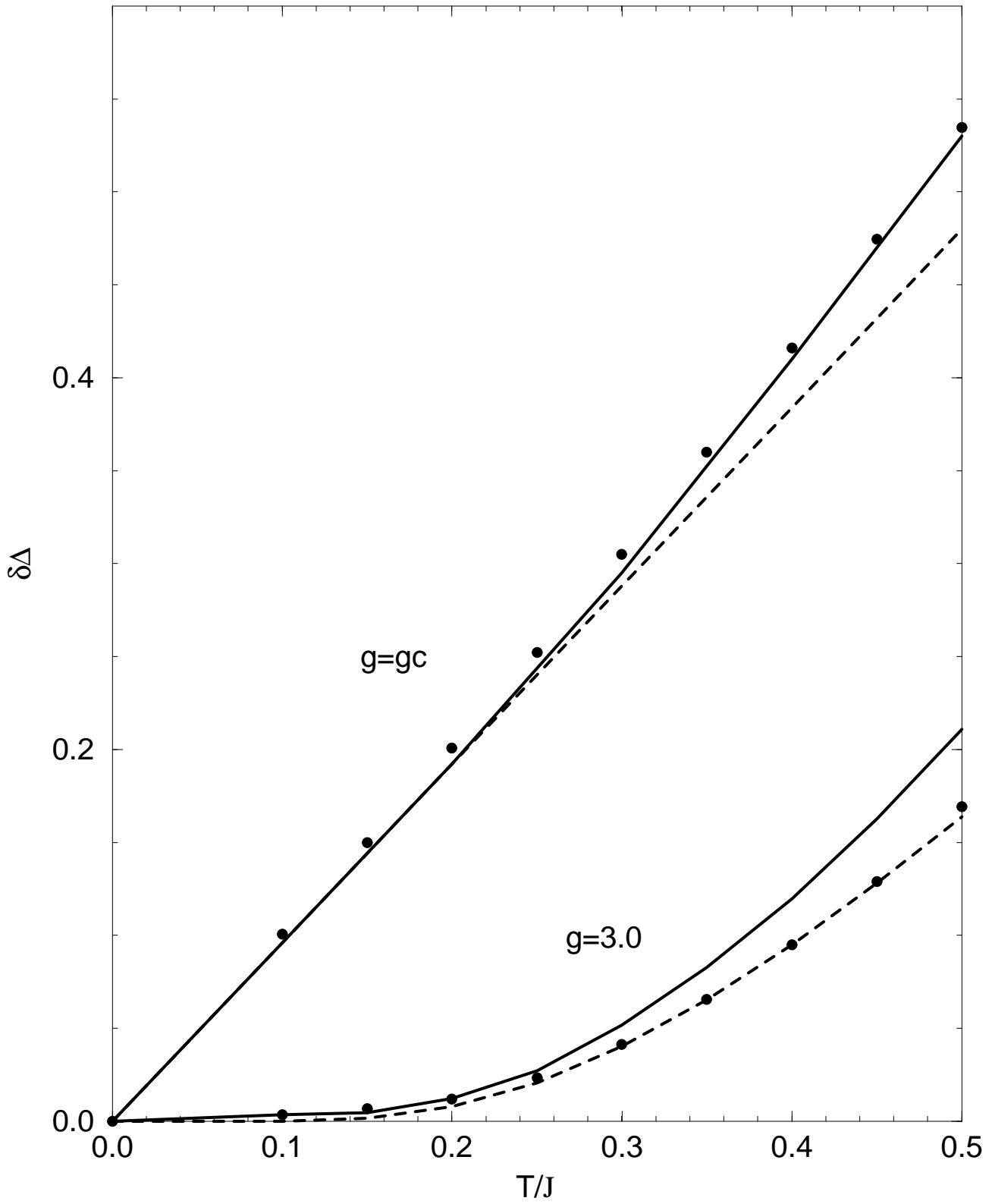


Fig.8

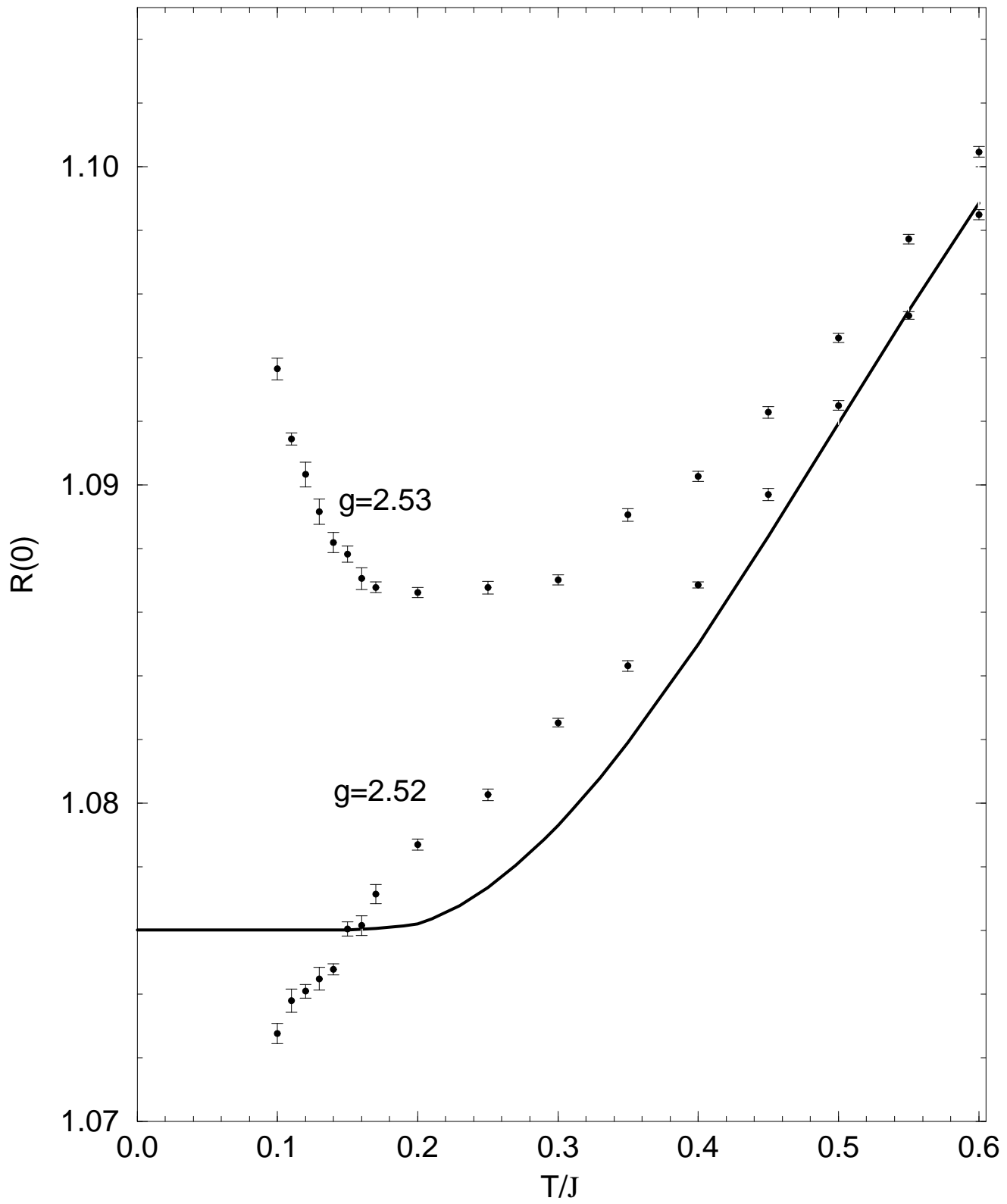


Fig.9

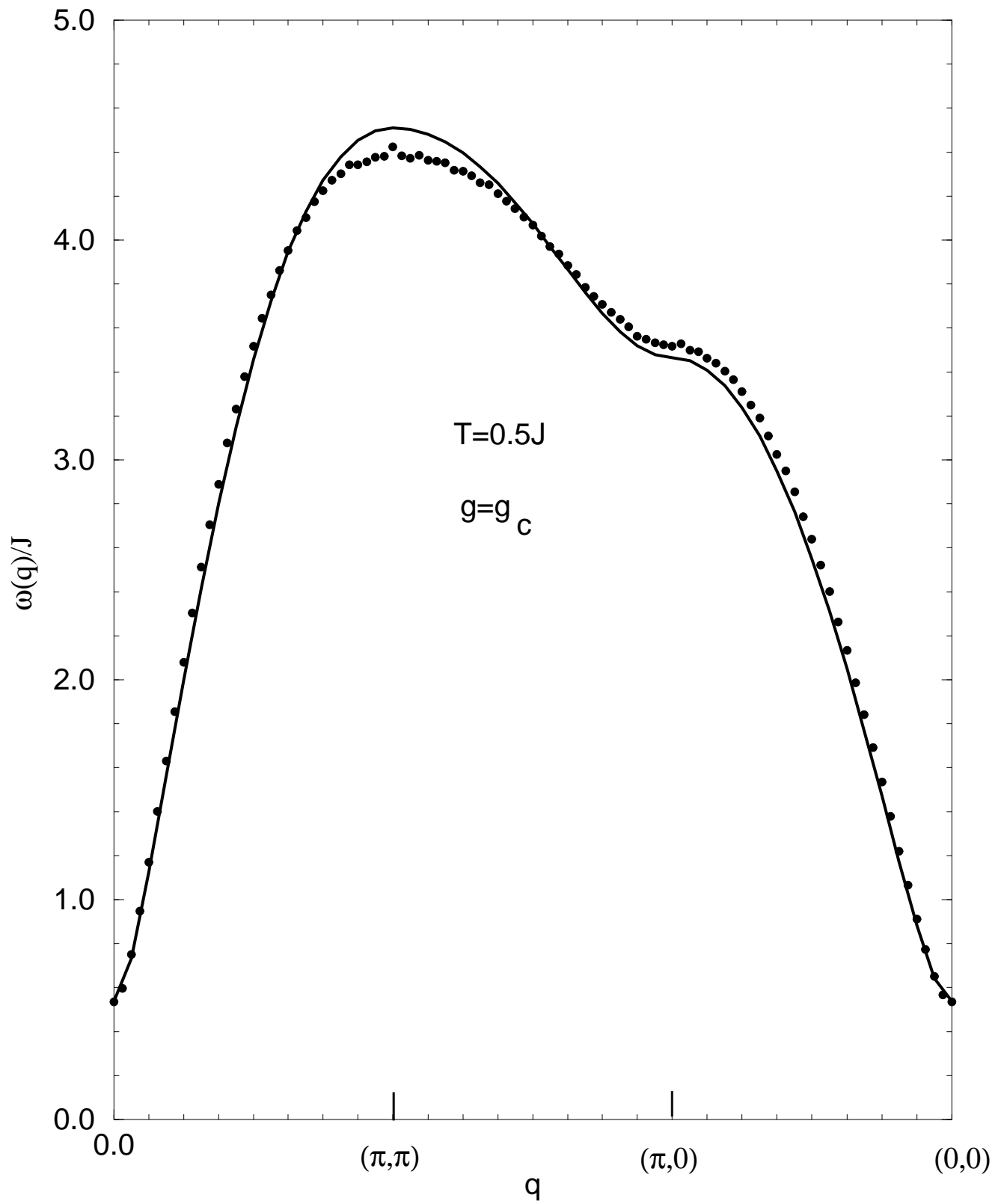
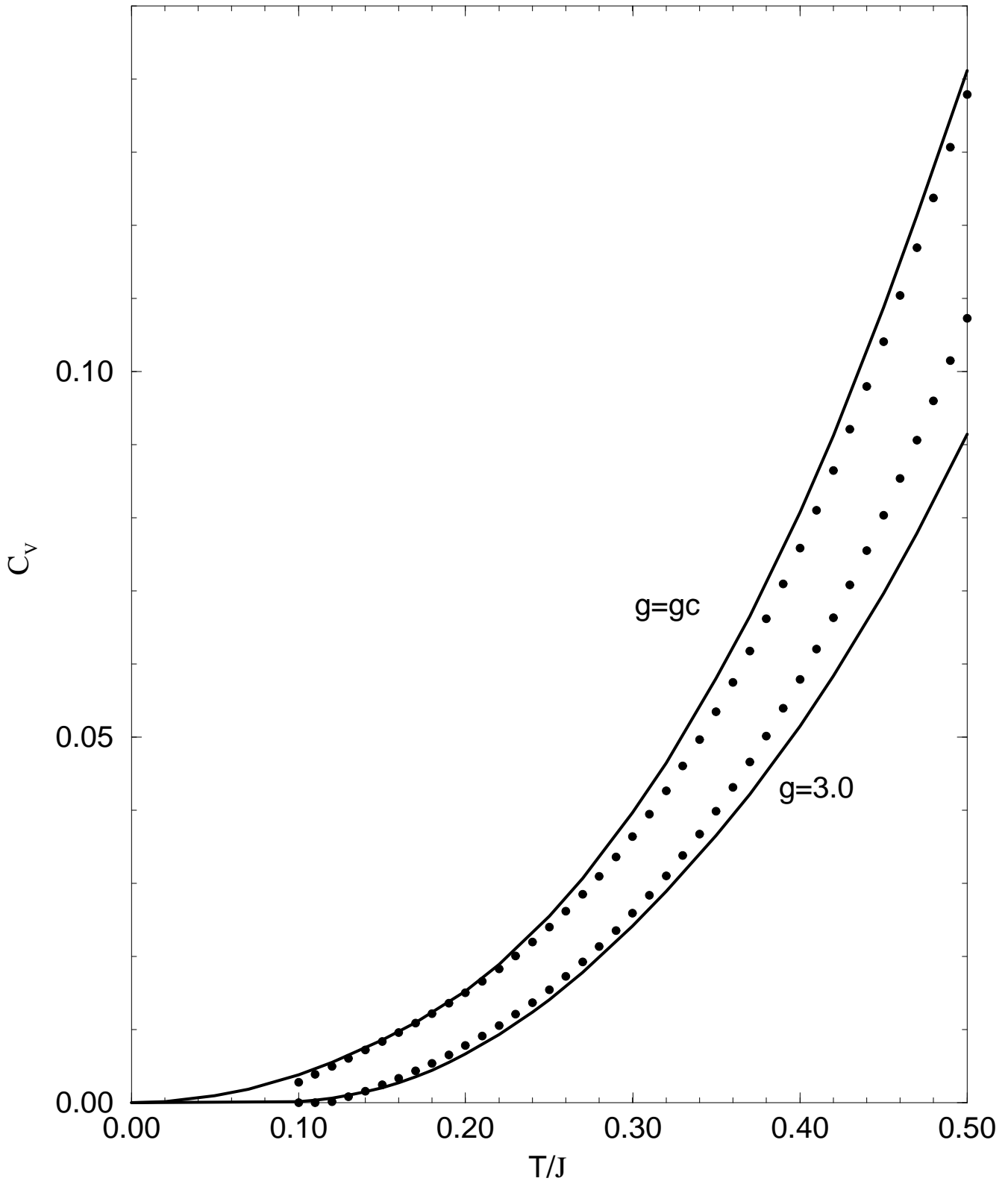
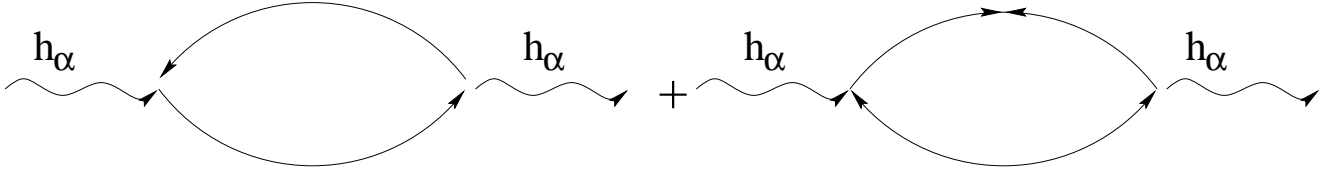


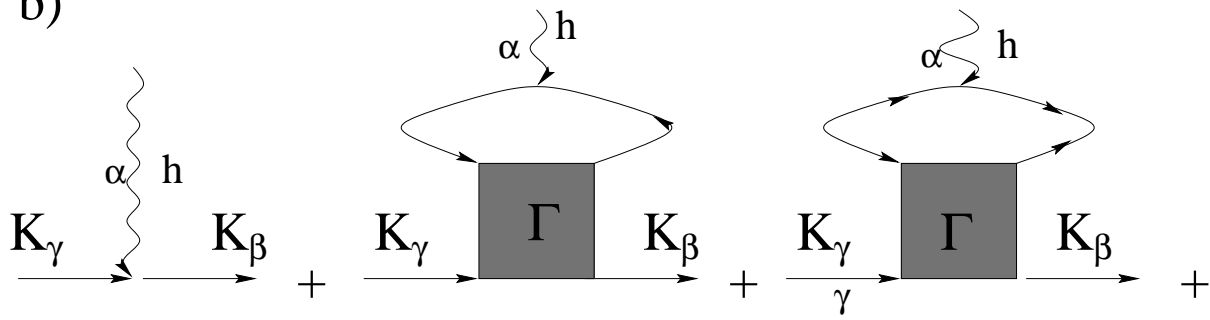
Fig.10



a)



b)



c)

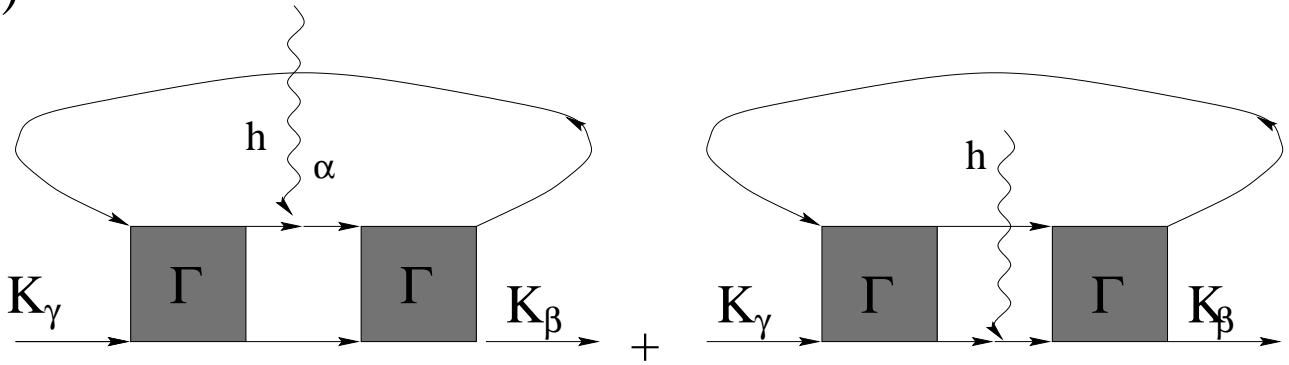


Fig.11

Fig.12

